UNIVERSIDADE FEDERAL DE MINAS GERAIS
FACULDADE DE MEDICINA
PROGRAMA DE PÓS-GRADUAÇÃO EM MEDICINA MOLECULAR

Matheus Felipe Guimarães Aguiar

EVALUATION OF THE GLIOSIS-REDUCING POTENTIAL OF CTK 01512-2, THE RECOMBINANT VERSION OF Phα1β TOXIN ISOLATED FROM THE VENOM OF *Phoneutria nigriventer*, IN A PARKINSON'S DISEASE MOUSE MODEL

Avaliação do potencial redutor de gliose da CTK 01512-2, versão recombinante da toxina Phα1β isolada do veneno de *Phoneutria nigriventer*, em modelo de Doença de Parkinson em camundongos

Belo Horizonte
2021

Matheus Felipe Guimarães Aguiar

EVALUATION OF THE GLIOSIS-REDUCING POTENTIAL OF CTK 01512-2, THE RECOMBINANT VERSION OF Phα1β TOXIN ISOLATED FROM THE VENOM OF *Phoneutria nigriventer*, IN A PARKINSON'S DISEASE MOUSE MODEL

Avaliação do potencial redutor de gliose da CTK 01512-2, versão recombinante da toxina Phα1β isolada do veneno de *Phoneutria nigriventer*, em modelo de Doença de Parkinson em camundongos

Dissertação apresentada ao Programa de Pós-Graduação em Medicina Molecular da Universidade Federal de Minas Gerais, como requisito parcial para obtenção de título de Mestre.

Orientador: Professor Marco Aurélio Romano Silva (MD-PhD)

Coorientador: Dr. Luiz Alexandre Viana Magno (PhD)

Belo Horizonte
2021

Aguiar, Matheus Felipe Guimarães.
AG282e Evaluation of the gliosis-reducing potential of CTK 01512-2, the recombinant version of Phα1β toxin isolated from the venom of Phoneutria nigriventer, in a Parkinson disease mouse model [manuscrito]. / Matheus Felipe Guimarães Aguiar. - - Belo Horizonte: 2021.
89f.: il.
Orientador (a): Marco Aurélio Romano-Silva.
Coorientador (a): Luiz Alexandre Viana Magno.
Área de concentração: Medicina Molecular.
Dissertação (mestrado): Universidade Federal de Minas Gerais, Faculdade de Medicina.

1. Oxidopamine. 2. Parkinson Disease. 3. Gliosis. 4. Doenças Neurodegenerativas. 5. Sistema Nervoso Central. 6. Dissertação Acadêmica. I. Romano-Silva, Marco Aurélio. II. Magno, Luiz Alexandre Viana. III. Universidade Federal de Minas Gerais, Faculdade de Medicina. IV. Título.

NLM: WL 359

Bibliotecário responsável: Fabian Rodrigo dos Santos CRB-6/2697

UNIVERSIDADE FEDERAL DE MINAS GERAIS
FACULDADE DE MEDICINA
PROGRAMA DE PÓS-GRADUAÇÃO EM MEDICINA MOLECULAR

FOLHA DE APROVAÇÃO

Avaliação do potencial redutor de gliose da CTK 01512-2, versão recombinante da toxina Phα1β isolada do veneno de *Phoneutria nigriventer*, em modelo de doença de Parkinson em camundongos

MATHEUS FELIPE GUIMARÃES AGUIAR

Dissertação de Mestrado defendida e aprovada, no dia vinte e oito de junho de dois mil vinte e um, pela Banca Examinadora designada pelo Colegiado do Programa de Pós-Graduação Medicina Molecular da Universidade Federal de Minas Gerais constituída pelos seguintes professores doutores:

Marco Aurelio Romano Silva - Orientador
UFMG

Luiz Alexandre Viana Magno - Coorientador
UNIFENAS

Helia Tenza Ferrer
UFMG

Marcus Vinicius Gomez
IEP-SCBH

Belo Horizonte, 28 de junho de 2021.

Documento assinado eletronicamente por **Helia Tenza Ferrer**, **Usuário Externo**, em 29/06/2021, às 13:40, conforme horário oficial de Brasília, com fundamento no art. 5º do Decreto nº 10.543, de 13 de novembro de 2020.

Documento assinado eletronicamente por **Marcus Vinicius Gomez**, **Usuário Externo**, em 29/06/2021, às 19:12, conforme horário oficial de Brasília, com fundamento no art. 5º do Decreto nº 10.543, de 13 de novembro de 2020.

Documento assinado eletronicamente por **Luiz Alexandre Viana Magno**, **Usuário Externo**, em 01/07/2021, às 14:12, conforme horário oficial de Brasília, com fundamento no art. 5º do Decreto nº 10.543, de 13 de novembro de 2020.

Documento assinado eletronicamente por **Marco Aurelio Romano Silva**, **Professor do Magistério Superior**, em 29/07/2021, às 11:19, conforme horário oficial de Brasília, com fundamento no art. 5º do Decreto nº 10.543, de 13 de novembro de 2020.

A autenticidade deste documento pode ser conferida no site https://sei.ufmg.br/sei/controlador_externo.php?acao=documento_conferir&id_orgao_acesso_externo=0, informando o código verificador **0801624** e o código CRC **8D5CF439**.

RESUMO

A resposta neuroinflamatória é importante para a recuperação da homeostase. Porém, em estado intenso e crônico, pode ser prejudicial ao Sistema Nervoso Central. Esforços para restringir os danos causados pela micróglia e os astrócitos, nesses casos, estão sendo investigados em doenças neurodegenerativas, uma vez que a reatividade excessiva dessas células poderia contribuir para o agravamento desses acometimentos. Aqui, mostramos a resposta da micróglia e dos astrócitos à degeneração dopaminérgica no estriado, em um modelo de camundongo com indução de doença de Parkinson por 6-OHDA, em seis momentos diferentes dentro de um período de seis meses. Além disso, descobrimos que uma única injeção intracerebroventricular de CTK 01512-2, versão recombinante de um peptídeo do veneno *Phoneutria nigriventer* capaz de inibir reversivelmente canais de cálcio, reduziu a reação severa da microglia e dos astrócitos na formação de cicatriz. Assim, como mostramos que o efeito anti-inflamatório da CTK 01512-2 poderia ser aplicada nos casos graves de gliose com formação de cicatriz, sugerimos que esse potencial deve ser melhor elucidado.

Palavras-chave: 6-OHDA, Doença de Parkinson, neuroinflamação, cicatriz glial, CTK 01512-2, Phα1β.

ABSTRACT

Neuroinflammatory response is important to recover the homeostasis, however in an intense and chronic state it could be harmful to the Central Nervous System. Efforts to restrict the microglia and astrocytes damage in these cases are being investigated in neurodegenerative diseases, since the excessive reactivity of these cells could contribute to the aggravation of these disorders. Here, we showed striatal microglia and astrocyte response to dopaminergic degeneration in a 6-OHDA Parkinson's disease mouse model, in six different moments within a six months window period. Furthermore, we found that a single intracerebroventricular injection of CTK 01512-2, a recombinant version of a *Phoneutria nigriventer* venom peptide that is capable of reversible inhibition of calcium channel, was able to reduce severe reaction of microglia and astrocytes in scar formation. Thus, as we showed that the CTK 01512-2 anti-inflammatory effect could be applied to severe cases of gliosis with scar formation, we suggest that this potential should be better elucidated.

Keywords: 6-OHDA, Parkinson’s disease, neuroinflammation, glial scar, CTK 01512-2, Phα1β.

LIST OF FIGURES

LIST OF FIGURES ON THE ARTICLE

LIST OF TABLES

TABLES ON THE ARTICLE

LIST OF ACRONYMS AND INITIALS

6-OHDA	6-hydroxydopamine
ACA	Anterior Commissure
AD	Alzheimer's Disease
ALS	Amyotrophic Lateral Sclerosis
AP	Anteroposterior
BBB	Blood-Brain Barrier
BSA	Bovine Serum Albumin
Ca^{2+}	Calcium
Ca_v	Voltage-gated Calcium Channel
CC	Corpus Callosum
CI	Confidence Interval
CNS	Central Nervous System
CP	Caudate Putamen
CT	Cylinder Test
DAT	Dopamine Transporter
DV	Dorsoventral
GFAP	Glial Fibrillary Acidic Protein
Iba1	Ionized Calcium Binding Adaptor Molecule 1
ICV	Intracerebroventricular Injection
K^+	Potassium
K_v	Voltage-gated Potassium Channel
LV	Lateral Ventricle
MD	Mean Difference
MedianD	Median Difference
ML	Mediolateral
MS	Multiple Sclerosis
Na^+	Sodium
NG2	Neuron-Glial Antigen 2
NO	Nitric Oxide
NSP	Nigrostriatal Projections

OFT	Open Field Test
PBS	Phosphate Buffer Solution
PD	Parkinson's Disease
PDGFRβ^{+}	Platelet-derived Growth Factor Receptor-beta
PFA	Paraformaldehyde
pH	Hydrogenionic Potential
ROI	Region Of Interest
ROS	Reactive Oxygen Species
S.E.M.	Standard Error of the Mean
SN	Substantia Nigra
SNc	Substantia Nigra Pars Compacta
StDM	Dorsomedial Striatum
TH	Tyrosine Hydroxylase

SUMMARY

1.0 INTRODUCTION

The immune system plays an important role in maintaining tissue homeostasis and responding to injuries and infections. Microglia is the main immune cell residing in the brain and spinal cord. In its basal state, it has a characteristic morphology and acts by reducing free radicals, cellular repair, and the release of anti-inflammatory factors, as well as performing phagocytosis. However, when it becomes responsive to a pathogen, changes or damage, it takes on a pro-inflammatory role that has the function of defending the tissue and initiating a repair process. This process, which is usually self-limiting, is extremely important to eradicate infections and restore tissue homeostasis. Cases where the inflammation is not controlled in a timely manner or the response is pronounced, there may be major harmful modifications to the tissue (GLASS et al., 2010; SOCHOCKA et al., 2017; ELLIS et al., 2018).

When active, microglia can proliferate, showing a different gene expression presenting morphological and surface channels alteration. This process, called microgliosis, could be considered neurotoxic, as it releases reactive oxygen species (ROS), nitric oxide (NO), proteases and pro-inflammatory cytokines, that in large quantities and in combination may lead to damage to the neurons, oligodendrocytes and extracellular matrix (KIM and VELLIS, 2005; BLOCK et al., 2006).

Astrocytes, the most abundant cell type in the mammalian brains, are involved in the regulation of neuronal activities through the tripartite synapse (presynaptic, postsynaptic neuron and the astrocyte), where it regulates the concentration of neurotransmitters, ions and pH homeostasis, and also participates, with the microglia, of the inflammatory process in the Central Nervous System (CNS) (ABBOTT et al., 2006; HALASSA et al., 2007). According to Sofroniew (2015), chronic degenerative processes, diffuse trauma, ischemia, and certain types of infection can cause severe astrogliosis. In these cases, the increase and activation of astrocytes, which occurs together with microglia and other cells, leads to a major reorganization of the tissue. Consequently, the potential for resolution and return to normal structure is reduced, which leads to the constant attempt of these cells to carry out the repair process.

Microglia produce factors that influence the microenvironment of astrocytes and neurons. The process that leads to “activation” of the microglia and its migration to the injury site are related to stimuli and assistance from astrocytes (DAVALOS et al., 2005; HAYNES et al., 2006). Thus, both cells play an important role together in controlling the inflammatory and reparative processes of the CNS. The

neuroinflammatory process is not necessarily responsible for initiating neurodegenerative diseases, still there is evidence that long-lasting inflammatory processes involving microglia and astrocytes contribute to the progression of these diseases (GLASS et al., 2010).

Neuroinflammation with scar formation is a complex system of interacting different cells. Two different areas can be identified in the mature lesion: (I) the penumbra area, presented on the periphery of the cells aggregate, which is formed by hypertrophic astrocytes, and (II) the center of this new tecidual organization, also known as the core, formed by the NG2 glia/oligodendrocyte precursor cells, meningeal and/or vascular derived fibroblasts (PDGFRβ$^+$), pericytes, ependymal cells, and phagocytic macrophages (**Figure 1**) (BUSH et al., 1999; FAULKNER et al.,

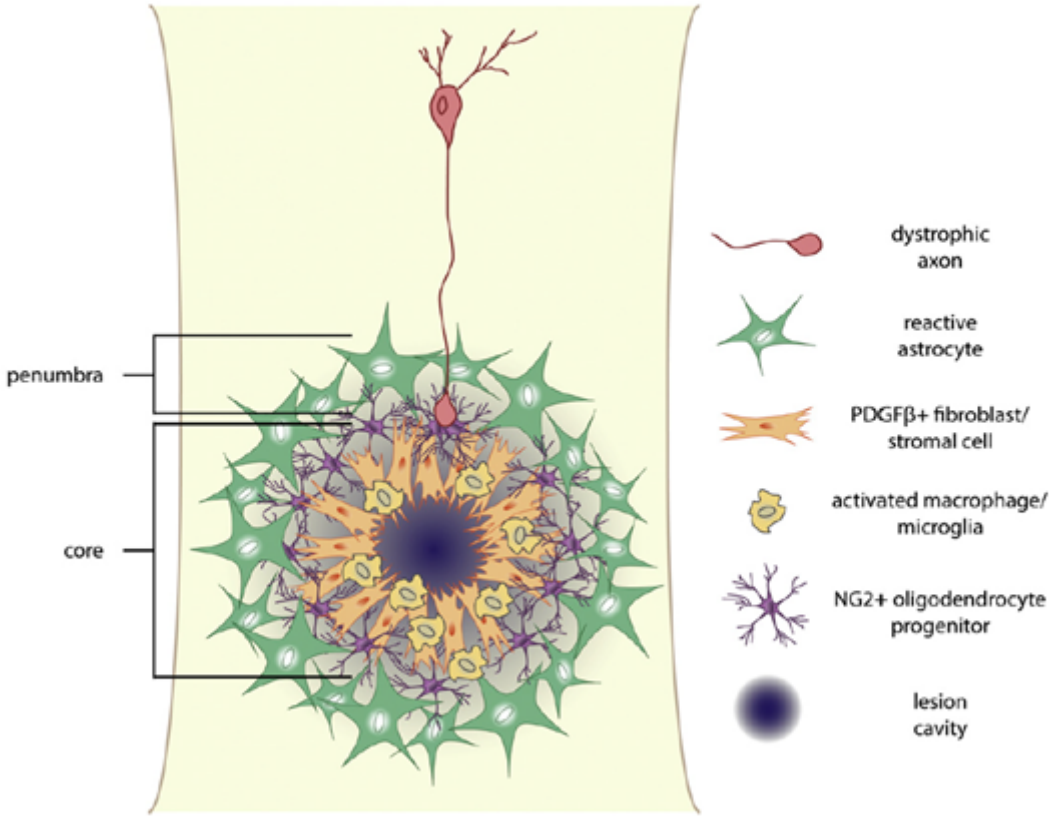

Figure 1. Glial scar organization. Representation of cell distribution on glial scar in CNS (here in spinal cord lesion). The penumbra region is composed of reactive astrocytes in hypertrophic form. The core of the lesion is formed by PDGFRβ$^+$ fibroblasts, macrophages/microglia, NG2$^+$ oligodendrocyte precursor cells. In the center, lesion cavities can be found. Adapted from Cregg et al., 2014.

2004; HORN et al., 2008; MELETIS et al., 2008; HERRMANN et al., 2008; SOFRENIEW et al., 2009; GÖRITZ et al., 2011; SODERBLOM et al., 2013;

WANNER et al., 2013). These studies suggest that the scar formed by glial cells prevents inflammatory processes from propagating to unaffected regions in the CNS, isolating the affected area.

Some studies have sought to identify the pattern of glia in CNS diseases and to see how they can enhance the damage that has occurred. In Alzheimer's disease (AD), it is possible to visualize around the senile plaques an alteraton in the morphology of the microglia, which changes from branched (basal state) to the ameboid state (“active”), and astrogliosis, identified by an increase in the number, size and mobility of astrocytes (AKIYAMA, 2000). In Parkinson's disease (PD), it is possible to observe the activation of microglia, and an increase in astrocytes (dystrophic), as well as an infiltration of lymphocytes (DAMIER et al., 1993; BRAAK et al., 2007). In Amyotrophic Lateral Sclerosis (ALS) it is possible to visualize a strong inflammatory reaction, which one of its characteristics is gliosis, with a large number of microglia and astrocytes in addition to the large production of cytotoxic substances and pro-inflammatory cytokines (MCGEER and MCGEER, 2002).

In order to study the molecular, biochemical and cellular mechanisms that affect these diseases, it is possible to use animal models with induced neurodegeneration. The 6-hydroxydopamine (6-OHDA) murine-injected model is one of the most used animal models, due to it is a great tool for screening possible neuroprotective agents (**Figure 2**) (KOSTRZEWA et al., 1974; NOELKER et al., 2005; LASTRES-BECKER et al., 2005; MCCOY et al., 2006; SEGURA-AGUILAR et al., 2015). 6-OHDA induces degeneration of dopaminergic neurons as it has a high affinity for the dopamine transporter (DAT) (GARVER et al., 1975). Once inside the cell, it enters the mitochondria and inhibits complex I and IV of the electron transport chain. This process causes defects in mitochondrial functioning and results in oxidative stress (GLINKA and YOUDIM, 1995). This is one of the main models for the study of PD: when injecting 6-OHDA into the striatal dopaminergic fibers, the nigrostriatal pathway enters the process of neurodegeneration (KOSTRZEWA et al., 1974; GARVER et al., 1975; SEGURA-AGUILAR et al., 2015).

The *Phoneutria nigriventer* spider, popularly known as the “armed spider”, has several potent toxins present in its venom (GOMEZ et al., 2002). The bite of this spider can cause severe pain, tremors, nausea, cramps, convulsions, profuse sweating, vomiting, excessive salivation, arrhythmias, visual disturbances, among other symptoms (LUCAS, 1988; BUCARETCHI et al., 2008; DE LIMA et al., 2015).

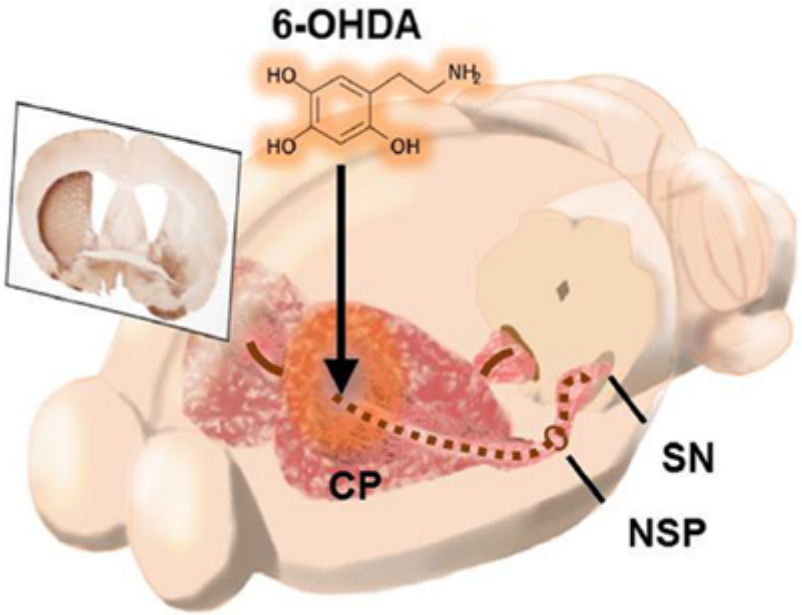

Figure 2. 6-hydroxydopamine Parkinson's disease mouse model. Representation of a mouse brain with an indication of 6-OHDA (chemical structure) injection on striatum (*caudate putamen* - CP). This leads to retrograde neurodegeneration of nigrostriatal projections (NSP), where the body of dopaminergic neurons are presented in *substantia nigra* (SN). Adapted from Becker et al., 2017.

Based on tests with intrathecal injections in animals and in symptoms found in humans, it was possible to notice that *P. nigriventer* venom has mainly neurotoxic effects (SUEUR et al., 2003; BUCARETCHI et al., 2008).

Several of the polypeptides presented in the venom interact with ion channels. In 1993, Arújo and collaborators demonstrated the interaction of a fraction of the *P. nigriventer* toxin over voltage-regulated sodium (Na^+) channels. Subsequently, it was observed that certain classes of these toxins act not only on the Na^+ channels, but also on calcium (Ca^{2+}), potassium (K^+), among others (GRISHIN, 1999; DE LIMA, 2015). The use of toxins present in the *P. nigriventer* venom demonstrated several pharmacologically promising effects, such as anti-arrhythmogenic effect in isolated rat hearts and in isolated ventricular cardiomyocytes (ALMEIDA et al., 2011), neuroprotective effects and reduction of cell death after induced process of ischemia in the hippocampus and retina (PINHEIRO et al., 2009; AGOSTINI et al., 2011), among other applications.

P. nigriventer toxins were initially named based on a gel filtration and reversed-phase chromatography (REZENDE et al., 1991). It was identified five distinct fractions, named PhTx1, PhTx2, PhTx3, PhTx4, and PhTx5 (**Figure 3**). Of all fractions, the PhTx3 is the most studied one, based on its pharmacological potential. These peptides interact with voltage-gated calcium channels (Ca_v) and voltage-gated potassium channels (K_v). This fraction has six toxins, identified as PnTx3-1 to PnTx3-6 (CASSOLA et al., 1998; CARDOSO et al., 2003).

The toxin PnTx3-6, patented under the name of Phα1β, is a peptide capable of reversibly blocking high Ca_v. It acts on N, R, P / Q, and L-type Ca_v channels, in that order of effectiveness (GOMEZ et al., 2002; VIEIRA et al., 2005). The biochemical and pharmacological characterization of the effects of toxins on physiological systems is of extreme interest. The use of this peptide has been extensively studied, using different models in acute, inflammatory, neuropathic, and cancer pain in rodents, and the results showed promising perspective of clinical use (SOUZA et al., 2008; RIGO et al., 2013a; RIGO et al., 2013b; TONELLO et al., 2014; ROSA et al., 2014; EMERICH et al., 2016; TONELLO et al., 2016; RIGO et al., 2017; TENZA-FERRER et al., 2019).

In addition to the analgesic effect, another possible application has called attention. Silva and colleagues (2015) reported that Phα1β showed the capacity to attenuate inflammatory events associated with hemorrhagic cystitis. In a mouse model of multiple sclerosis (MS) it was found an improvement in the neuroinflammatory responses (SILVA et al., 2018). Tenza-Ferrer and others (2019) found that the blockade of Ca^{2+} by this peptide was able to act in reactive astrocytes and microglia, suggesting the use as a potent anti-inflammatory compound on glial cells.

To avoid scarcity and improve availability on application, the recombinant version of this peptide was created, annotated as CTK 01512-2. Several studies showed that the recombinant version has similar effects to the native peptide (SOUZA et al., 2008; TONELLO et al., 2017; RIGO et al., 2017; SILVA et al., 2018; ANTUNES et al., 2020), and some of these studies have already used only the CTK in their investigation, including the study of Silva and colleagues (2018).

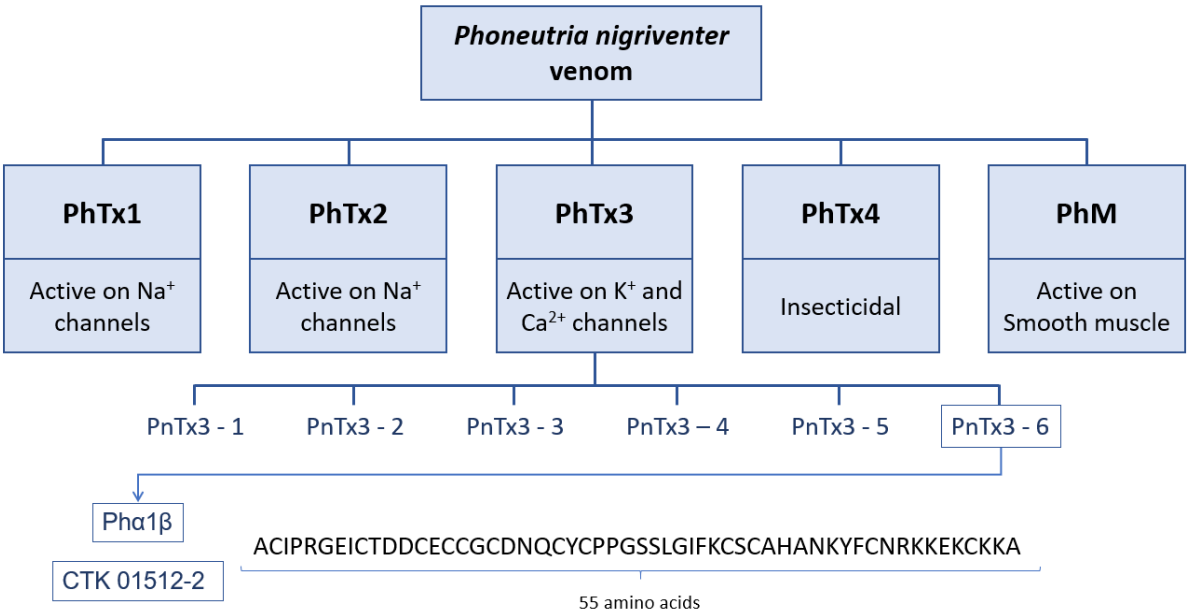

Figure 3. Phα1β extracted from *P. nigriventer* venom. Flowchart showing the distribution of *Phoneutria nigriventer* venom fractions (PhTx and PhM), and the toxins of PhTx3 (PnTx3-1 to PnTx3-6). The fraction 6 was named Phα1β and its recombinant version, CTK 01512-2, both having the same amino acid structure. Adapted from DE LIMA et al., 2016.

Studies with peptides derived from *P. nigriventer* venom represent not only a possibility for pharmacological use, but a possibility to apply them as a tool to have a better understanding of physiological function and the functioning of ion channels. Therefore, here we present a longitudinal evaluation of microglia and astrocytes response to a dopaminergic neurodegeneration, and the effect of CTK, the recombinant version of Phα1β, under the time point with greater glial reactivity.

2.0 OBJECTIVES

2.1 Overall Objectives

Investigate the response of the astrocytes and microglial cells to dopaminergic neurodegeneration caused by 6-OHDA, and verify whether CTK 01512-2 is able to reduce or prevent astrogliosis and microgliosis in the striatum.

2.2. Specific Objectives

Study the inflammatory response of astrocytes and microglia over time in the 6-OHDA model of Parkinson's disease.

Assess whether CTK infusion would be able to reverse or mitigate the initial motor changes caused by unilateral dopaminergic depletion.

Determine if the administration of CTK influences the dopaminergic neurodegeneration process.

Verify whether CTK alters the process of astrocytic and microglial reactivity.

3.0 ARTICLE

The calcium channel blocker CTK 01512-2 reduces neuroinflammatory scar in a mouse model of Parkinson's Disease.

3.1 ABSTRACT

Neuroinflammatory response is important to recover the homeostasis, however in an intense and chronic state it could be harmful to the Central Nervous System. Efforts to restrict the microglia and astrocytes damage in these cases are being investigated in neurodegenerative diseases, since the excessive reactivity of these cells could contribute to the aggravation of these disorders. Here, we showed striatal microglia and astrocyte response to dopaminergic degeneration in a 6-OHDA Parkinson's disease mouse model, in six different moments within a six months window period. Furthermore, we found that a single intracerebroventricular injection of CTK 01512-2, a recombinant version of a *Phoneutria nigriventer* venom peptide, capable of reversible inhibition of calcium channel, was able to reduce severe reaction of microglia and astrocytes in scar formation. Thus, as we showed that the CTK 01512-2 anti-inflammatory effect could be applied to severe cases of gliosis with scar formation, we suggest that this potential should be better elucidated.

Keywords: 6-OHDA Parkinson's disease mouse model, neuroinflammation, glial scar, CTK 01512-2, Phα1β.

3.2 INTRODUCTION

The immune system plays an important role in maintaining tissue homeostasis and in responding to injuries and infections. Microglia is the main immune cell residing in the brain and spinal cord. When it becomes responsive to a pathogen, changes or damage, it has the function of defending the tissue and initiating a repairing process (GLASS et al., 2010; SOCHOCKA et al., 2017). Astrocytes, involved directly on the regulation of neuronal activities through the tripartite synapse (presynaptic, postsynaptic neuron and the astrocyte), together with the microglia, are the mainly responsible cells of the inflammatory process in the Central Nervous

System (CNS) (ABBOTT et al., 2006; HALASSA et al., 2007).

In chronic degenerative processes, the increase and activation of astrocytes, which occurs together with microglia and other cells, leads to a major reorganization of the tissue. The potential for resolution and return to normal structure of the brain tissue is reduced, promoting the constant attempt of these cells to carry out the repair process. This could lead to damage to the neurons, oligodendrocytes and extracellular matrix (KIM and VELLIS, 2005; BLOCK et al., 2006; SOFRONIEW et al., 2015). This usually causes a glial scar formation, a complex system of interacting different cells, which assumes a distribution at the site of the injury to restore tissue homeostasis and prevent inflammatory processes from spreading to unaffected regions of the CNS, isolating the affected area (BUSH et al., 1999; FAULKNER et al., 2004; HORN et al., 2008; MELETIS et al., 2008; HERRMANN et al., 2008; SOFRENIEW et al., 2009; GÖRITZ ET AL., 2011; SODERBLOM et al., 2013; WANNER et al., 2013).

Studies have sought to identify the pattern of glia in neurodegenerative diseases and to see how they can enhance the damage that has occurred. In Parkinson's disease (PD), it is possible to observe the activation of microglia, and an increase in astrocytes (dystrophic), as well as an infiltration of lymphocytes (DAMIER et al., 1993; BRAAK et al., 2007).

Peptides extracted from animal venoms have called attention to their perspective to research and therapeutic use. The *Phoneutria nigriventer* spider, popularly known as the “armed spider”, has several potent toxins present in its venom (GOMEZ et al., 2002). The toxin PnTx3-6, patented under the name of Phα1β, is a peptide capable of reversibly blocking N, R, P/Q and L-type high voltage-gated calcium channels (Ca_v), in that order of effectiveness (GOMEZ et al., 2002; VIEIRA et al., 2005). The use of this peptide has been extensively studied, using different models in acute, inflammatory, neuropathic and cancer pain in rodents, and the results showed promising perspective of clinical use (SOUZA et al., 2008; RIGO et al., 2013a; RIGO et al., 2013b; TONELLO et al., 2014; ROSA et al., 2014; EMERICH et al.,2016; OLIVEIRA et al., 2016; TONELLO et al., 2016; RIGO et al., 2017). In addition to the analgesic effect, another possible application has called attention, the anti-inflammatory effect. Attenuation of inflammatory events associated with hemorrhagic cystitis (SILVA et al., 2015), reduction of the neuroinflammatory responses in a mouse model of multiple sclerosis (SILVA et al., 2018), and action on

reactive astrocytes and microglia on an inflammatory process on spinal cord (TENZA-FERRER et al., 2019) were stated. This raises the matter of how this anti-inflammatory effect occurs and which situations it could be applied.

To avoid scarcity and improve availability on application, the recombinant version of this peptide was made, annotated as CTK 01512-2. Several studies showed that the recombinant version has similar effects to the native peptide and some of these studies have already used exclusively the CTK in their investigation (SOUZA et al., 2008; TONELLO et al., 2017; RIGO et al., 2017; ANTUNES et al., 2020).

Studies with peptides derived from venom represent not only a possibility for pharmacological use, but a possibility to use them as a tool to have a better understanding of physiological function and ion channels activity.

In the present study, we performed a longitudinal microscopic evaluation of microglia and astrocytes response to the 6-hydroxydopamine (6-OHDA) Parkinson's disease mouse model, in different time points over six months. After a single intracerebroventricular injection (ICV) of CTK, the recombinant version of Phα1β, in the time point with greater glial reactivity, we identified reduction of microglia and astrocyte scar formation, caused by dopaminergic neurodegeneration on striatum.

3.3 MATERIALS AND METHODS

3.3.1 Animals

Male and female C57BL/6 mice were used, aged 7-8 weeks of life (18-20g). The animals were housed in facilities with controlled temperature (22 ± 1 °C), 12h light/dark schedule and water and food ad libitum. The procedures were approved by the Ethics Committee on the Use of Animals (CEUA) of the Federal University of Minas Gerais (UFMG), under the protocol number 322/2019.

3.3.2 Surgical procedures

Mice were anesthetized with intraperitoneal injection of ketamine/xylazine (80mg/kg per 8 mg/kg), and were maintained under deep anesthesia throughout the surgery with a mixture of oxygen (1.0 L/min) and isoflurane at 1%. They were placed into a stereotaxic frame with body temperature controlled by a feedback heating pad (David

Kopf Instruments). Using a dental drill with a 0.75mm burr, craniotomy was done in one or two coordinates. Injections were made by a pulled glass micropipette (Nanoliter 2010, World Precision Instruments).

Unilateral dopamine depletion

The 6-OHDA craniotomy was made according to the following coordinates: anteroposterior (AP) 0.5mm from bregma, mediolateral (ML) 2.0mm, and dorsoventral (DV) -3.0mm. PBS injection, used as control in the experiment to characterize the glial response, followed the same coordinates but in the left hemisphere. Aliquots of 6-OHDA-HBr (Sigma-Aldrich) were dissolved in ice-cold 0.02% ascorbic acid in sterile phosphate buffer solution (PBS) (w/v) at a concentration of 4µg/µl. The volume injected was 1200nl at a rate of 100nl/min with 5 min for diffusion.

Intracerebroventricular injection (ICV)

This procedure was made right after induction of unilateral dopaminergic depletion. For the ICV injection, the coordinates to the right lateral ventricle were: AP -0.25mm, ML 1.0mm, and DV -2.15mm. CTK 01512–2, the recombinant version of Phα1β (Giotto Biotech®) at 50 pmol/injection or vehicle (PBS) was injected through a pulled glass micropipette with a single injection of 1500nl at a rate of 200nl/min. CTK stock solutions were prepared to the required concentration on the day of the surgery. During the 7 postsurgical days, mice were allowed free access to sugared water (10 mM) and food pellets soaked in kitten milk replacement to stimulate appetite and gastrointestinal motility. During this period, we also administered daily 0.5 ml of lactated Ringer's solution (subcutaneously) to avoid dehydration (MAGNO et al., 2019a).

3.3.3 Behavioral testing

Mice were submitted to analysis of spontaneous locomotor activity seven days before the surgery to injection of 6-OHDA and ICV, and seven days after these procedures. Animals were placed individually and habituated for 30 min before the test.

Cylinder test (CT): assessed in 10 min sessions, mice were placed into a non-reflective glass cylinder with 20 cm height and 9 cm diameter (MAGNO et al., 2019b).

Open field test (OFT): In an open field box with 40 cm long, 40 cm wide, and 50 cm deep, mice were recorded for 10 min.

Distance traveled, average speed, time immobile and spontaneous rotations were scored using automated video-tracking software (ANY-maze version 6.3, Stoelting). Rotational behavior (full 360° turns) was expressed as the percentage of ipsilateral (6-OHDA injection side) or contralateral rotations relative to the total number of rotations over the period of testing. Data were analyzed as repeated measures (pre-post).

3.3.4 Histology

Mice were anesthetized with intraperitoneal ketamine/xylazine (100 mg/kg per 10 mg/kg body weight) injection and transcardially perfused with ice-cold saline (0.9%) followed by freshly prepared 4% paraformaldehyde in PBS (pH 7.4). Brains were postfixed for 12 h in 4% PFA at 4°C. Using a vibrating blade microtome (Leica Microsystems; Wetzlar, Hesse, Germany) coronal 50 µm slices were prepared. A mouse brain atlas (Franklin and Paxinos, 2008) was used to choose representative coronal sections surrounding the 6-OHDA injection site of the striatum. Slices were washed with PBS and incubated with permeabilizing-blocking solution (PBS with 4% BSA and 0.2% Triton X-100) for 1h30 at room temperature and and incubated overnight at 4°C in the same solution containing the primary antibodies at the indicated dilutions: anti-Iba1 (Wako, catalog# 019-19741, RRID:AB_839504, 1:500), GFAP (Sigma-Aldrich, catalog# G3893, RRID:AB_477010, 1:500), anti-tyrosine hydroxylase (Abcam, catalog# ab76442, RRID:AB_1524535, 1:1000). Slices were washed in PBS and incubated for 3 hours with following AlexaFluor dye-conjugated secondary antibodies: AF-488 anti-rabbit (Thermo Fisher, catalog# A11008, RRID:AB_143165, 1:1,000), AF-594 anti-mouse (Thermo Fisher, catalog# A11005, RRID:AB_2534073, 1:1,000) and AF-488 anti-chicken (Thermo Fisher, catalog# A11039, RRID:AB_2534096, 1:1,000) (MAGNO et al., 2020). After that, slices were washed and mounted in Dako fluorescent mounting medium (Agilent Technologies, CA, United States). Three dimensional z stacks were acquired using a SP5 confocal microscope (Leica Microsystems; Wetzlar, Hesse, Germany), keeping settings constant in each experiment for comparison between mice. Images were captured under 10X objective, resolution of 1,024 X 1,024 pixels and 100 HZ speed. Iba1 manual countage, GFAP and TH fluorescent intensity were evaluated under individual maximum z-projections with a delimitation of as region of interest (ROI). All

images were analyzed in Fiji/ImageJ software version 1.53c (SCHNEIDER et al., 2012).

3.3.5 Statistics

Results are expressed as mean ± S.E.M. for all measures. Normality was tested using Shapiro–Wilk normality test ($\alpha < 0.05$) to determine whether parametric or nonparametric analyses were required. The statistical significance of differences between groups was assessed using an unpaired Student's t-test or Mann-Whitney test, two-way ANOVA followed by Tukey's multiple comparison tests or repeated measures two-way ANOVA followed by Tukey's multiple comparison tests, and one-way ANOVA followed by Tukey's. For the exact number of animals used in each experiment and details of statistical analyses, see the figure legend. All statistical analysis was performed using Prism version 5 (GraphPad Software).

3.4 RESULTS

3.4.1 Neurodegeneration caused by 6-OHDA induces microglial response

Since its characterization, 6-OHDA is considered a toxin capable of inducing nigrostriatal neurodegeneration (UNGERSTEDT et al., 1968). Therefore, 6-OHDA-Parkinson's disease mouse model is extremely used to investigate neuroprotection, neurorepair, pharmacological strategies, and glial response to this process (CICCHETTI et al., 2002; MARIN et al., 2007; WALSH et al., 2011; PARRA et al., 2019).

To characterize microglial response to the neurodegeneration, we injected 6-OHDA on the right hemisphere and PBS on the left, and evaluated six different time points: 3 hours, 24 hours, 3 days, 7 days, 3 months and 6 months, in five subregions of the dorsal striatum, in the AP coordinates: +0.86mm, +0.50mm, +0.26mm, +0.14mm and -0.22mm (**Figure 1** and **Figure 2A**. Representative images of AP +0.26mm are in the **Supplementary Figure 1**). It was not observed changes in the number of $Iba1^+$ cells in the 3-hour group, when compared between the hemisphere injected with 6-OHDA and PBS, in any of the five coordinates (mean difference (MD): 0.86: -0.0037, 95% CI -0.03841 to 0.04578, $t_{(6)} = 0.2142$, $p = 0.8375$; 0.50: 0.0384, 95% CI -0.1303 to 0.05356, $t_{(6)} = 1.022$, $p = 0.3464$; 0.26: 0.0117, 95%

CI -0.03329 to 0.009746, $t_{(5)}$ = 1.406, p = 0.2186; 0.14: 0.0481, 95% CI -0.1393 to 0.04303, $t_{(6)}$ = 1.292, p = 0.2439; -0.22: 0.008, 95% CI -0.09063 to 0.07462, $t_{(6)}$ = 0.2371, p = 0.8204, Student's *t*-test; **Figure 2B**). In the 24-hour group, we found an increase in the number of Iba1^{+} cells within the injection of 6-OHDA only on the anterior regions analyzed (0.86: 0.0646, 95% CI -0.1111 to -0.01817, $t_{(6)}$ = 3.403, p = 0.0144; 0.50: 0.1099, 95% CI -0.2101 to -0.009655, $t_{(6)}$ = 2.683, p = 0.0364; 0.26: 0.0672, 95% CI -0.1187 to -0.01574, $t_{(6)}$ = 3.195, p = 0.0187; 0.14: 0.083, 95% CI -0.1898 to 0.02388, $t_{(6)}$ = 1.900, p = 0.1061; -0.22: -0.0293, 95% CI -0.06631 to 0.1142, $t_{(6)}$ = 0.6488, p = 0.5405, Student's *t*-test; **Figure C**). In the 3-day group we observed significant changes on AP +0.86mm, +0.50mm, but not in +0.26mm (0.86: 0.0776, 95% CI -0.1301 to -0.02517, $t_{(6)}$ = 3.621, p = 0.0111; 0.50: 0.1085, 95% CI -0.1759 to -0.04121, $t_{(6)}$ = 3.945, p = 0.0076; 0.26: 0.0784, 95% CI -0.1655 to 0.008609, $t_{(6)}$ = 2.205, p = 0.0696, Student's *t*-test; **Figure 2D**). The striatal subregions at AP +0.14mm and -0.22mm of the 3-day group as well as the 7-day

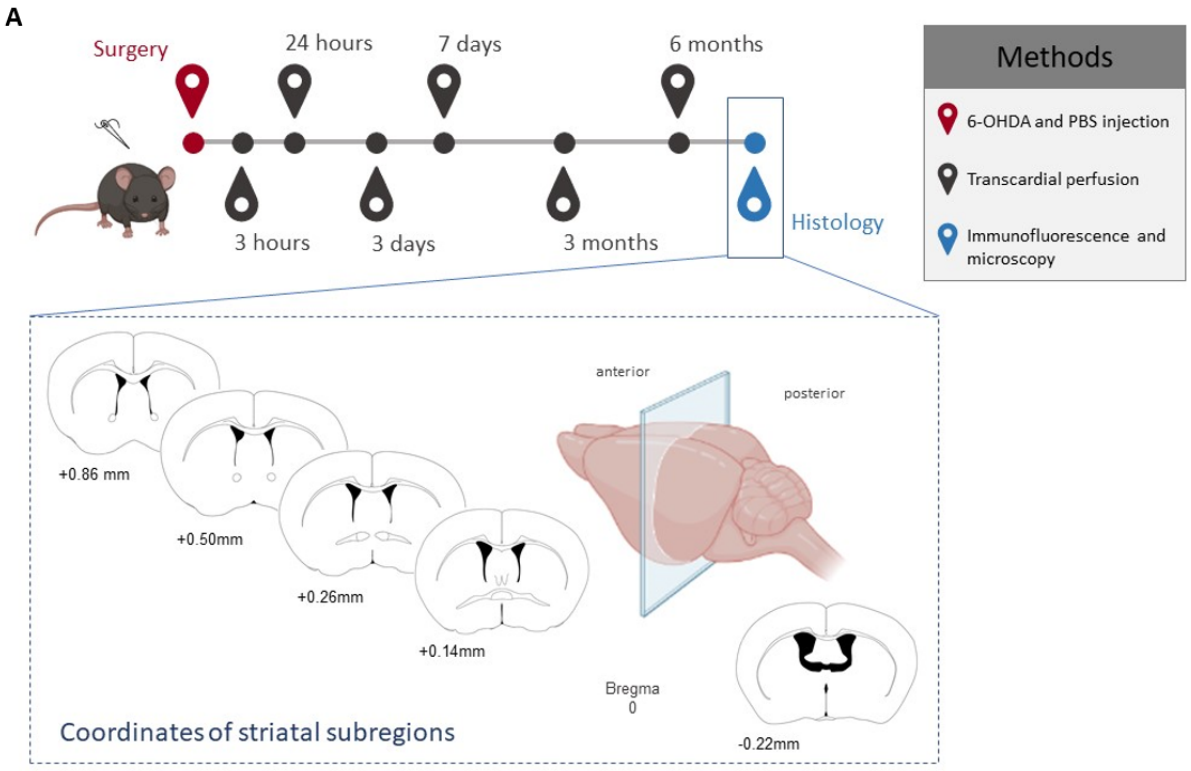

Figure 1. Experimental design to assess gliosis in the Parkinson's disease mouse model. (A) Experimental design of the induction of dopaminergic neurodegeneration (Parkinson's disease mouse model). The animals received an injection of 6-OHDA in the right hemisphere and PBS in the left. The tissue was collected 3 hours, 24 hours, 3 days, 7 days, 3 months or 6 months after surgery. For histology purposes, 5 coordinates from the AP axis, containing striatal subregions, were analyzed.

group were not analyzed, since the scar formation made cell quantification unviable. The 3- and 6-month group did not demonstrate significant changes on Iba1^{+} number between the hemispheres in any of the points evaluated (3 months: 0.86: 0.0384, 95% CI -0.1472 to 0.07038, $t_{(4)}$ = 0.9802, p = 0.3825; 0.50: 0.0434, 95% CI -0.09365 to 0.006720, $t_{(4)}$ = 2.405, p = 0.0740; 0.26: 0.0011, 95% CI -0.1145 to 0.1124, $t_{(4)}$ = 0.02563, p = 0.9808; 0.14: 0.0861, 95% CI -0.2083 to 0.03622, $t_{(4)}$ = 1.954, p = 0.1224; -0.22: 0.1079, 95% CI -0.2517 to 0.03594, $t_{(4)}$ = 2.083, p = 0.1057; 6 months: 0.86: 0.0279, 95% CI -0.08242 to 0.02656, $t_{(4)}$ = 1.423, p = 0.2278; 0.50: 0.0515, 95% CI -0.1184 to 0.01537, $t_{(4)}$ = 2.138, p = 0.0993; 0.26: 0.0381, 95% CI -0.1939 to 0.1178, $t_{(4)}$ = 0.6780, p = 0.5349; 0.14: 0.0548, 95% CI -0.1337 to 0.02409, $t_{(4)}$ = 1.929, p = 0.1260; -0.22: 0.0906, 95% CI -0.1813 to 0.0001377, $t_{(4)}$ = 2.772, p = 0.0502; Student's *t*-test; **Figure 2E-F**).

When comparing the same striatal subregions between time points, to identify the difference intergroups, all of them demonstrated a significant difference (two-way ANOVA with Tukey's multiple comparison test, groups: 0.86: $F_{(4,\ 26)}$ = 27.82, p <0.0001; 0.50: $F_{(4,\ 26)}$ = 12.36, p < 0.0001; 0.26: $F_{(4,\ 26)}$ = 3.487, p = 0.0208; 0.14: $F_{(3,\ 20)}$ = 6.945, p = 0.0022; -0.22: $F_{(3,\ 20)}$ = 8.675, p = 0,0007, two-way ANOVA; **Figure 2G-K; Supplementary tables 1**).

Evaluating the overall result of the striatum (average of the 5 coordinates: +0.86mm to -0.22mm) by time point, the 24-hour, 3-day, 3- and 6-month groups showed an increase of the number of microglia on the hemisphere injected with 6-OHDA, when compared with PBS side (two-way ANOVA with Tukey's multiple comparison test, groups: $F_{(4,\ 36)}$ = 41.35, p < 0.0001; 3-hour: MD: 0.01781, 95% CI -0.02506 to 0.06069, $t_{(36)}$ = 1.126, p = 0.7891; 24-hour: MD: 06016; 95% CI 0.01728 to 0.1030, $t_{(36)}$ = 3.804, p = 0.0027; 3-day: MD: 0.08820, 95% CI 0.03285 to 0.1436, $t_{(36)}$ = 4.320, p = 0.0006; 3-month: MD: 0.05537, 95% CI 0.01250 to 0.09825, $t_{(36)}$ = 3.501, p = 0.0063; 6-month: MD: 0.05258, 95% CI 0.009702 to 0.09546, $t_{(36)}$ = 3.325, p = 0.0102; **Figure 2L; Supplementary tables 2**). When we took in consideration only +0.86mm, +0.50mm and +0.26mm, regions closer to the injection site, only 24-hour and 3-day groups exhibited an increase of Iba1^{+} on the 6-OHDA side (two-way ANOVA with Tukey's multiple comparison test, groups: $F_{(4,\ 26)}$ = 28.87, p < 0.0001; 3-hour: MD: 0.01097, 95% CI -0.03769 to 0.05963, $t_{(26)}$ = 0.6246, p = 0.9789; 24-hour: MD: 08058; 95% CI 0.03192 to 0.1292, $t_{(26)}$ = 4.587, p = 0.0005; 3-day: MD: 0.08820, 95% CI 0.03954 to 0.1369, $t_{(26)}$ = 5.021, p = 0.0002; 3-month: MD: 0.02764,

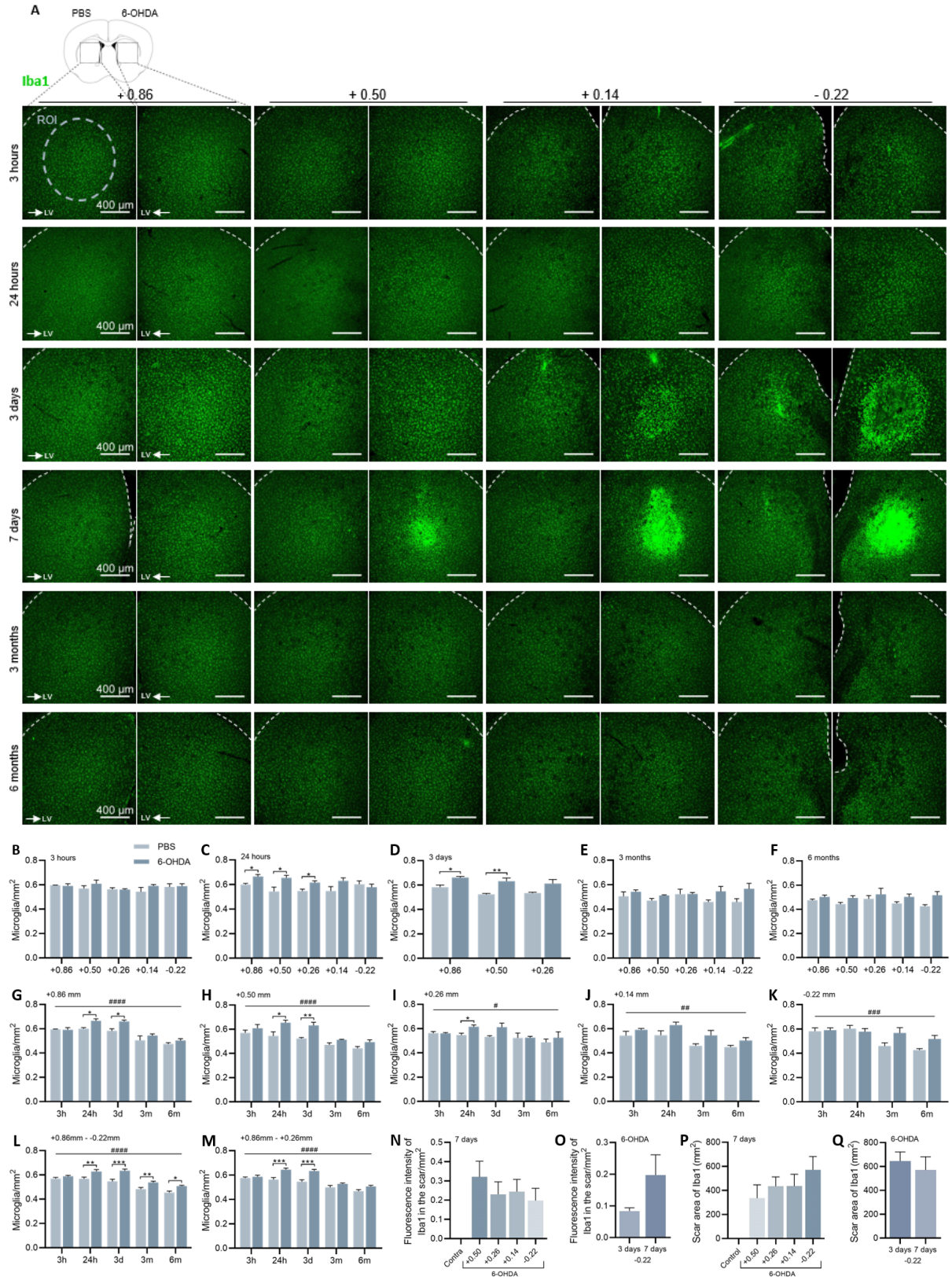

Figure 2. Microglial response to dopaminergic neurodegeneration in the dorsal striatum. (A) Representative coronal images of Iba1-labeled microglia (Iba1^{+}) in the dorsal striatum, showing the 6-OHDA (left) and PBS (right) injection sides of the AP coordinates +0.86, +0.50, +0.14 and -0.22, in the 6 groups (3 hours, 24 hours, 3 days, 7 days, 3 months or 6 months). **(B, C, D, E, F)** Quantification of Iba1^{+} between the coordinates +0.86, +0.50, -0,26, +0.14 and -0.22, and between hemispheres in the 3 hour-group **(B)**, 24 hour-group **(C)**, 3

(*Continued*)

Figure 2. Continued

(G, H, I, J, K) Quantification of Iba1$^+$ inter-hemispheres and intergroups in the AP +0.86mm **(G)**, +0.50mm **(H)**, +0.26mm **(I)**, +0.14mm **(J)**, -0.22 **(K)**. **(L, M)** Inter-hemispheres and intergroup analyses of microglia of the average of the striatal subregions at AP +0.86mm, +0.50mm +0.26mm, +0.14mm and -0.22 (except in the 3-day group) **(L)** or only in the average of the AP coordinates +0.86mm, +0.50mm +0.26mm, the ones closer to the injection site **(M)**. **(N)** Fluorescence intensity within the scar in the 7-day group. **(O)** Analysis of the fluorescence intensity within the scar between the 6-OHDA injected hemispheres of -0.22 of the group of 3 and 7 days. **(P)** Measurement of the scar area in the 7 day-group and **(Q)** at -0.22 in the 3- and 7-day groups. Data represented as mean ± S.E.M. (n = 3-4/group). ***P < 0.001, **P < 0.01, *P < 0.05, when compared between hemispheres of the same group (PBS and 6-OHDA). #### P < 0.0001, ### P < 0.001, ## P < 0.01, #P < 0.05, when compared between all groups. LV: Lateral Ventricle.

95% CI -0.02855 to 0.08383, $t_{(26)}$ = 1.363, p = 0.6397; 6-month: MD: 0.03916, 95% CI -0.01703 to 0.09535, $t_{(26)}$ = 1.931, p = 0.2835; **Figure 2M; Supplementary tables 3**).

In an inflammatory process where scar formation by glial cells occurs, it is possible to identify different areas in the mature lesion. The microglia migrates for the central area, the core, together with NG2 glia/oligodendrocyte precursor cells, pericytes, ependymal cells, and others (BUSH et al., 1999; FAULKNER et al., 2004; HORN et al., 2008; MELETIS et al., 2008; HERRMANN et al., 2008; SOFRONIEW et al., 2009; GÖRITZ ET AL., 2011; SODERBLOM et al., 2013; WANNER et al., 2013).

The scar formation, observed only in the 6-OHDA injection side, started to be noted 3 days after injection, and in the 7-day group is presented in more regions than in the previous time point (**Figure 2B**). This process did not cause a significant difference in the fluorescence of Iba1$^+$ in the region of the scar between the AP coordinates on the seventh day (one-way ANOVA with Tukey's multiple comparison test, subregions: $F_{(3,\ 13)}$ = 0.5504, p = 0.6567; **Figure 2N**). The fluorescence of the scar, compared between 3- and 7-day groups on -0.22mm did not exhibit a significant difference (-0.22: MD: 0.11374, 95% CI -0.04462 to 0.2721, $t_{(6)}$ = 1.757, p = 0.1294, Student's *t*-test; **Figure 2O**). The scar formed by the microglia seemed to be growing and better limited anteroposteriorly, but this did not cause a significant change in the area, between the slices of the 7-day group, not even when we compared the scar area between the 3- and 7-day on -0.22mm (one-way ANOVA with Tukey's multiple comparison test, 7 days: subregions: $F_{(3,\ 13)}$ = 0.8698, p < 0.4816; **Figure 2P;** -0.22: MD: -74.9, 95% CI -404.6 to 255.0, $t_{(6)}$ = 0.5550, p = 0.5989, Student's *t*-test; **Figure 2Q**).

Thus, we showed that microglia reacted to the 6-OHDA injection as soon as 24 hours after the procedure. We also demonstrated that scar formation started 3

days after 6-OHDA injection, and it was better established 7 days after the procedure, when it was the most advanced point of microgliosis amongst the time points we evaluated. Lastly, we observed a decline in microgliosis process in the 3- and 6-months groups.

3.4.2 Neurodegeneration caused by 6-OHDA induces astrocyte response

We also verified the response of astrocytes to the effect of 6-OHDA. Under CNS injury, astrocytes assume a hypertrophic form, with an intense production of cytoskeleton filaments, including the intermediate filaments called glial fibrillary acidic protein (GFAP). On a scar formation, they create a barrier on the periphery, called penumbra zone (BUSH et al., 1999; SOFRONIEW et al., 2009; WANNER et al., 2013).

Assessing fluorescence intensity of GFAP, that is upregulated in reactive astrocytes, we identified that in 3- and 24-hour groups the reaction and production of this protein was not enough to have GFAP-positive cells on striatum (**Figure 3A**). However, we observed an increase of fluorescence, in the hemisphere injected with 6-OHDA, in the posterior AP subregions of the striatum after 24 hours, which was not seen in the 3-hour group (3 hours: 0.86: MD 0.0, 95% CI -0.1365 to 0.1365 , $t_{(6)}$ = 3.136, p = 0.9999; 0.50: -0.017, 95% CI -0.1014 to 0.1354, $t_{(6)}$ = 0.3507, p = 0.7378; 0.26: -0.0469, 95% CI -0.08639 to 0.1801, $t_{(6)}$ = 0.8605, p = 0.4226; 0.14: -0.0225, 95% CI -0.2232 to 0.2681, $t_{(6)}$ = 0.2238, p = 0.8303; -0.22: -0.0878, 95% CI -0.2472 to 0.4236, $t_{(6)}$ = 0.6432, p = 0.5439; 24 hours: 0.86: 0.1242, 95% CI -0.3923 to 0.1431, $t_{(6)}$ = 1.139, p = 0.2982; 0.50: 0.1962, 95% CI -0.4999 to 0.1069, $t_{(6)}$ = 1.585, p = 0.1640; 0.26: 0.2831, 95% CI -0.5380 to -0.02896, $t_{(6)}$ = 2.725, p = 0.0344; 0.14: 0.2894, 95% CI -0.5099 to -0.06935, $t_{(6)}$ = 3.217, p = 0.0182; -0.22: 0.368, 95% CI -0.6384 to -0.09632, $t_{(6)}$ = 3.316, p = 0.0161, Student's *t*-test; **Figure B-C**). Three days after 6-OHDA injection, we verified the presence of GFAP reactive astrocytes and also the beginning of the astrocyte scar formation, which we observed only in the more posterior region. Then, the fluorescence was higher in the hemisphere where 6-OHDA was injected in all points (0.86: 0.7616, 95% CI -1.204 to -0.3205, $t_{(6)}$ = 4.223, p = 0.0055; 0.50: 0.9164, 95% CI -1.431 to -0.4028, $t_{(6)}$ = 4.365, p = 0.0047; 0.26: 0.856, 95% CI -1.473 to -0.2380, $t_{(6)}$ = 3.390, p = 0.0147; 0.14: 0.7229, 95% CI -1.259 to -0.1871, $t_{(6)}$ = 3.301, p = 0.0164; -0.22: 0.972, 95% CI -1.830 to -0.1135, $t_{(6)}$ = 2.770, p = 0.0324, Student's *t*-test; **Figure D**). On the seventh day, we also

observed an increase of fluorescence in the hemisphere injected with 6-OHDA, when compared with the PBS side, and the scar extended to more anterior regions. The PBS side did not show scar formation, only reactivity to lesion caused by the injection. (0.86: 1.2089, 95% CI -1.637 to -0.7806, $t_{(8)}$ = 6.509, p = 0.0002; 0.50: 1.086, 95% CI -1.604 to -0.5683, $t_{(8)}$ = 4.837, p = 0.0013; 0.26: 0.991, 95% CI -1.450 to -0.5317, $t_{(8)}$ = 4.976, p = 0.0011; 0.14: 0.93, 95% CI -1.560 to -0.3005, $t_{(8)}$ = 3.407, p = 0.0093; -0.22: 0.986, 95% CI -1.798 to -0.1744, $t_{(8)}$ = 2.802, p = 0.0231, Student's *t*-test; **Figure E**). After 3 and 6 months, the decrease in fluorescence we observed between hemispheres was no longer noted. $GFAP^+$ astrocytes were verified in -0.22mm in the center of the scar site, which was previously filled by the microglia, but this did not cause a significant difference in the fluorescence inter-hemispheres (3 months: 0.86: -0.0405, 95% CI -0.3149 to 0.3984, $t_{(4)}$ = 0.3149, p = 0.7686; 0.50: -0.0301, 95% CI -0.2410 to 0.3012, $t_{(4)}$ = 0.3080, p = 0.7734; 0.26: 0.0487, 95% CI -0.3583 to 0.2610, $t_{(4)}$ = 0.4364, p = 0.6851; 0.14: 0.0569, 95% CI -0.2557 to 0.1420, $t_{(4)}$ = 0.7938, p = 0.4718; -0.22: 0.316, 95% CI -0.6631 to 0.02968, $t_{(4)}$ = 2.539, p = 0.0641, Student's *t*-test; 6 months: 0.86: MedianD -0.0524, p = 0.4000; 0.50: MedianD 0.1445, p > 0.9999; 0.26: 0.0204, 95% CI -0.6700 to 0.6289, $t_{(4)}$ = 0.08781, p = 0.9343; 0.14: 0.246, 95% CI -0.8087 to 0.3227, $t_{(4)}$ = 1.139, p = 0.22989; -0.22: MedianD 0.3136, p = 0.4000, Student's *t*-test or Mann-Whitney; **Figure F-G**).

When comparing the same subregion among the time points evaluated, all of them demonstrated an intergroup significant difference (two-way ANOVA with Tukey's multiple comparison test, subregions: 0.86: $F_{(5, 36)}$ = 9.381, p < 0.0001; 0.50: $F_{(5, 34)}$ = 9.191, p < 0.0001; 0.26: $F_{(5, 34)}$ = 8.417, p < 0.0001; 0.14: $F_{(5, 34)}$ = 6.333, p = 0.0003; -0.22: $F_{(5, 34)}$ = 4.473, p = 0.0031, two-way ANOVA; **Figure 3H-L; Supplementary tables 4**).

When we assessed the average of the 5 striatal subregions in the 3- hour, 24-hour, 3-, 7-day, 3- and 6-month groups, the increase of fluorescence in the 6-OHDA-hemisphere was significant, and even without the precise identification of the astrocytes in the 24-hour group an intergroup difference was observed (two-way ANOVA with Tukey's multiple comparison test, groups: $F_{(5, 34)}$ = 38.19, p < 0.0001; 3-hour: MD: -0.03489, 95% CI -0.2659 to 0.1961, $t_{(34)}$ = 0.4219, p = 0.9988; 24-hour: MD: 0.2523; 95% CI 0.02131 to 0.4833, $t_{(34)}$ = 0.4219, p = 0.0261; 3-day: MD: 0.8458, 95% CI 0.6148 to 1.077, $t_{(34)}$ = 10.23, p <0.0001; 7-day: MD: 1.040, 95% CI 0.8338 to 1.247, $t_{(34)}$ = 10.06, p <0.0001; 3-month: MD: 0.07031, 95% CI -0.1964 to

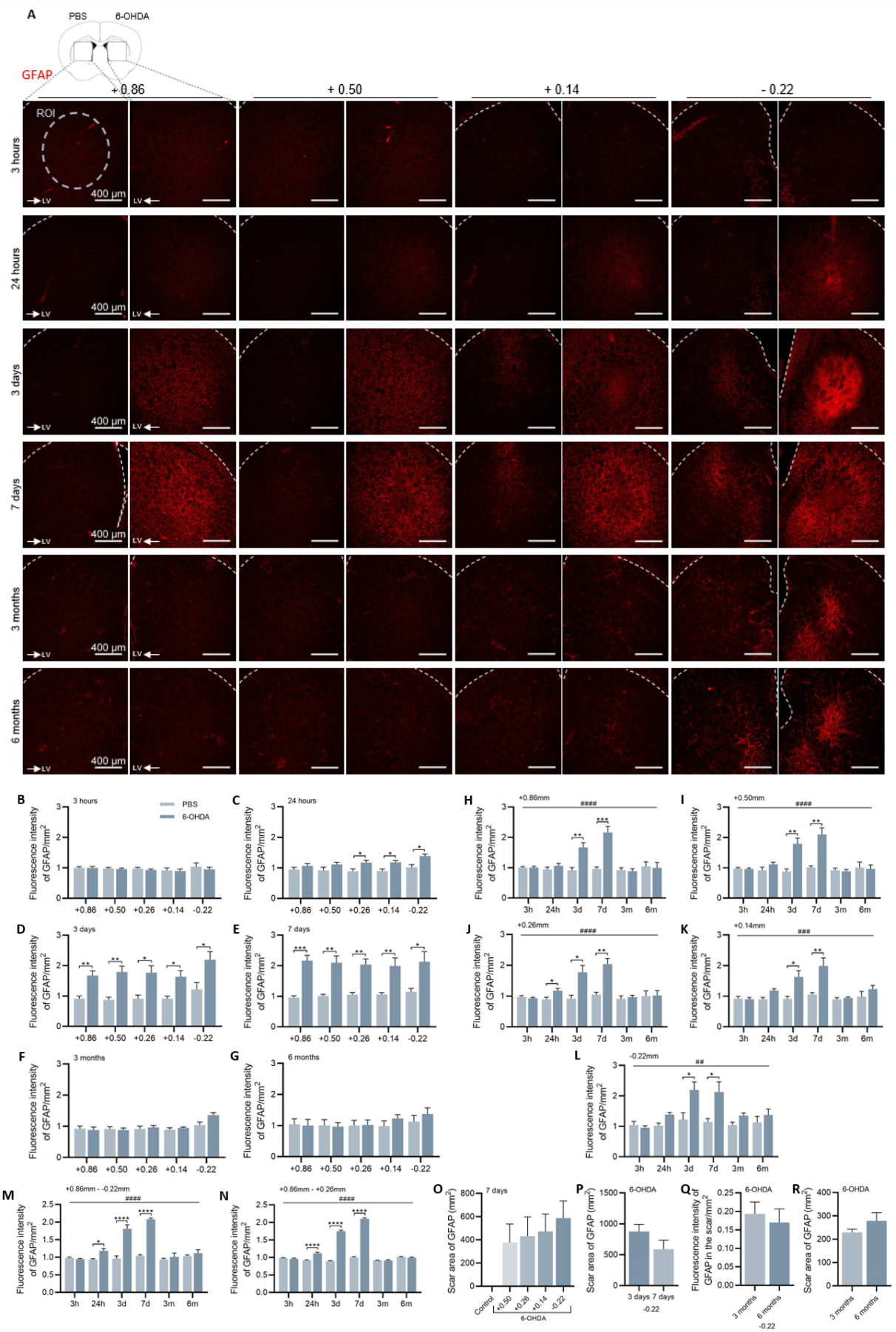

Figure 3. Astrocytes response to dopaminergic neurodegeneration in the dorsal striatum. (*continued*)

Figure 3. Continued

(A) Representative coronal images of GFAP-labeled astrocytes (GFAP$^+$) in the dorsal striatum, showing the PBS (left) and 6-OHDA (right) injection sides of the coordinates AP +0.86, +0.50, +0.14 and -0.22, in the 6 groups. **(B, C, D, E, F, G)** Quantification of GFAP$^+$ fluorescence the striatal subregions at +0.86, +0.50, -0,26, +0.14 and -0.22 between hemispheres in the 3 hour-group **(B)**, 24 hour-group **(C)**, 3 day-group **(D)**, 7 day-group **(E)**, 3 month-group **(F)** and 6 month-group **(G)**. **(H, I, J, K, L)** Quantification of GFAP$^+$ fluorescence between hemispheres and between groups at AP +0.86 **(H)**, +0.50 **(I)**, +0.26 **(J)**, +0,14 **(K)**, -0,22 **(L)**. **(M, N)** Inter-hemispheres and intergroup analyses of microglia of the average of the coordinates +0.86mm, +0.50mm +0.26mm, +0.14mm, -0.22 **(M)**, or only in the average of the coordinates AP +0.86mm, +0.50mm +0.26mm, the ones closer to the injection site **(N)**. **(O)** Measurement of the scar area in the striatal subregions of the 7-day group, and **(P)** at -0.22 of the 3- and 7-day group. **(Q)** Analysis of the fluorescence intensity within the scar between the ipsi-hemispheres (6-OHDA) of AP -0.22 of the group of 3 and 6 months, and **(R)** scar area. Data represented as mean ± S.E.M. (n = 3-4/group). ***P < 0.001, **P < 0.01, *P < 0.05, when compared between hemispheres of the same group (PBS and 6-OHDA). #### P < 0.0001, ### P < 0.001, ## P < 0.01, #P < 0.05, when compared between all groups. LV: Lateral Ventricle.

0.3371, $t_{(34)}$ = 0.7362, p = 0.9770; 6-month: MD: 0.08298, 95% CI -0.1838 to 0.3497, $t_{(34)}$ = 0.8689, p = 0.9490; **Figure 3M; Supplementary tables 5**). Restricting the amount of the regions to the interval closest to the injection site (AP +0.86mm, +0.50mm and +0.26mm) the difference in the fluorescence between hemispheres is even greater in the 24-hour group (two-way ANOVA with Tukey's multiple comparison test, groups: $F_{(5, 34)}$ = 302.5, p < 0.0001; 3-hour: MD: -0.02128, 95% CI -0.1047 to 0.06219, $t_{(34)}$ = 0.7119, p = 0.9805; 24-hour: MD: 0.02989; 95% CI 0.1181 to 0.2850, $t_{(34)}$ = 6.744, p <0.0001; 3-day: MD: 0.8448, 95% CI 0.7613 to 0.9282, $t_{(34)}$ = 28.27, p <0.0001; 7-day: MD: 1.095, 95% CI 1.021 to 1.170, $t_{(34)}$ = 40.98, p <0.0001; 3-month: MD: -0.007328, 95% CI -0.1037 to 0.08906, $t_{(34)}$ = 0.2123, p >0.9999; 6-month: MD: -0.02169, 95% CI -0.1181 to 0.07469, $t_{(34)}$ = 0.6286, p = 0.9897; **Figure 3N; Supplementary tables 6**).

The area of evacuation of the astrocytes in the 7-day group seemed to grow from the front to the back on the AP axis, but this difference was not statistically significant (one-way ANOVA with Tukey's multiple comparison test, subregions: $F_{(3, 12)}$ = 0.2905, p = 0.8314; **Figure 3O**), and this also happened when we compared the scar area on AP -0.22mm between 3- and 7-day groups (-0.22: MD: -288.5, 95% CI -746.3 to 169.1, $t_{(6)}$ = 1.543, p = 0.1738, Student's *t*-test; **Figure 3P**).

After that, we assessed whether there was a difference in the intensity of fluorescence and in the area of the astrocytes aggregate that occurred at 3- and 6 months, and that was not observed (-0.22: fluorescence: MD: -0.0233, 95% CI -0.1589 to 0.1123, $t_{(4)}$ = 0.4770, p = 0.6583; area: MedianD: 5.4, p = 0.4000, Student's *t*-test or Mann-Whitney; **Figure 3Q-R**).

Together, these results showed that reactive astrocytes were observed clearly 3 days after 6-OHDA injection, already showing the scar organization. Seven days after the procedure, the scar was better limited and extended more widely on striatal AP subregions. In 3- and 6-month groups, we observed a decline in $GFAP^+$ cells, since we did not see them in all coordinates, and in these time points the reactive astrocytes were occupying the center of where the inflammatory process was located at first.

3.4.3 CTK treatment did not improve initial motor dysfunction and the dopaminergic neurodegeneration

In the unilateral 6-OHDA injection mouse model, after a certain level of dopaminergic neurodegeneration, the animals display a forelimb akinesia (reduction of the capacity to execute a movement) of the paw impaired with the lesion site. Therefore, a 6-OHDA injection on the right hemisphere would cause an impairment of the left forelimb, with preference for rotation and vertical exploration with the right paw (OLSON et al., 1995; KIRIK et al., 1998; MAGNO et al., 2019a).

We injected mice unilaterally with 6-OHDA (unilateral dopamine-depleted mice), and a group received intracerebroventricular (ICV) injection of CTK, and the other of PBS. Motor function was assessed before and after 7 days of the neurodegeneration induction and PBS or CTK ICV injection (**Figure 4A**). Even at a moderate degeneration phase, it was possible to identify alterations on the motor behavior between pre- and post-depletion on the cylinder test (CT), but no significant difference was identified between the groups for distance travelled (two-way repeated-measure ANOVA, time: $F_{(1,\ 13)} = 24.83$, $p = 0.0003$; treatment: $F_{(1,\ 13)} = 0.8236$, $p = 0.6033$; **Figure 4B**), average speed (two-way repeated-measure ANOVA, time: $F_{(1,\ 13)} = 24.38$, $p = 0.0003$; treatment: $F_{(1,\ 13)} = 0.3114$, $p = 0.5863$; **Figure 4C**), and time immobile (two-way repeated-measure ANOVA, time: $F_{(1,\ 13)} = 52.14$, $p < 0.0001$; treatment: $F_{(1,\ 13)} = 0.4841$, $p = 0.4988$; **Figure 4D**). Evaluating the preference of the direction of rotation, it was possible to identify the characteristic rotation to the ipsilateral (6-OHDA) side, with no difference between groups (two-way repeated-measure ANOVA, time: $F_{(1,\ 13)} = 8.090$, $p = 0.0138$; treatment: $F_{(1,\ 13)} = 0.03713$, $p = 0.8502$; **Figure 4E**). On the open field test (OFT), there was also no difference between the groups, only changes in motor behavior after surgery, with a reduction in the distance travelled (two-way repeated-measure ANOVA, time: $F_{(1,\ 13)} =$

100.8, p <0.0001; treatment: $F_{(1, 13)}$ = 2.627, p = 0.1291; **Figure 4F**), average speed (two-way repeated-measure ANOVA, time: $F_{(1, 13)}$ = 100.3, p < 0.0001; treatment: $F_{(1, 13)}$ = 2.583, p = 0.1320; **Figure 4G**), and increase in time immobile (two-way repeated-measure ANOVA, time: $F_{(1, 13)}$ = 21.99, p = 0.0004; treatment: $F_{(1, 13)}$ = 3.218, p = 0.0961; **Figure 4H**). The animals also showed preference for rotations to the ipsi side, but with no significant difference between groups (two-way repeated-measure ANOVA, time: $F_{(1, 13)}$ = 57.59, p < 0.001; treatment: $F_{(1, 13)}$ = 0.3341, p = 0.5731; **Figure 4I**).

The immunoreactivity of the dopaminergic fibers on the striatum demonstrated a significant reduction in the fluorescence of tyrosine hydroxylase (TH) in the hemisphere injected with 6-OHDA when compared with the control side after 7 days (**Figure 5A**). This was observed along all the striatal subregions analyzed, individually or with the average of the four coordinates, in both groups (PBS: 0.86: -0.02882, 95% CI 0.01155 to 0.04609, $t_{(6)}$ = 4.084, p = 0.0065; 0.50: -0.02484, 95% CI 0.008667 to 0.04100, $t_{(6)}$ = 3.759, p = 0.0094; 0.14: -0.02656, 95% CI 0.005658 to 0.04747, $t_{(5)}$ = 3.266, p = 0.0223; -0.22: -0.02282, 95% CI 0.005302 to 0.04033, $t_{(6)}$ = 3.188, p = 0.0189, 0.86 to -0.22 (average): MedianD -0.02407, p = 0.0571; CTK: 0.86: -0.02096, 95% CI 0.007056 to 0.03488, $t_{(6)}$ = 3.688, p = 0.0102; 0.50: -0.02024, 95% CI 0.01136 to 0.02913, $t_{(6)}$ = 5.576, p = 0.0014; 0.14: -0.01805, 95% CI 0.01020 to 0.02590, $t_{(6)}$ = 5.629, p = 0.0013; -0.22: -0.01517, 95% CI 0.009195 to 0.02115, $t_{(6)}$ = 6.210, p = 0.0008; 0.86 to -0.22 (average): -0.01861, 95% CI 0.009845 to 0.02737, $t_{(6)}$ = 5.195, p = 0.0020, Student's t-test or Mann-Whitney; **Figure 5B-C**).

Comparing the side with neurodegeneration between the groups with different treatments, no significant difference was found on the anterior subregions, only in the more posterior points. No significant change was found on the average of the four subregions of the striatum (PBSxCTK: 0.86: -0.00027, 95% CI -0.004524 to 0.003969, $t_{(6)}$ =0.1598, p = 0.8783; 0.50: 0.00008, 95% CI -0.003050 to 0.003207, $t_{(6)}$ = 0.06145, p = 0.9530; 0.14: -0.00042, 95% CI -0.004602 to 0.003750, $t_{(6)}$ = 0.2496, p = 0.8112; -0.22: -0.00337, 95% CI -0.006630 to -0.0001138, $t_{(6)}$ = 2.532, p = 0.0445; 0.86 to -0.22 (average): MedianD -0.00026, p = 0.4857, Student's t-test or Mann-Whitney; **Figure 5D**). In the control hemisphere, we found no significant difference (PBSxCTK: 0.86: -0.00813, 95% CI -0.02989 to 0.01363, $t_{(6)}$ =0.9143, p =

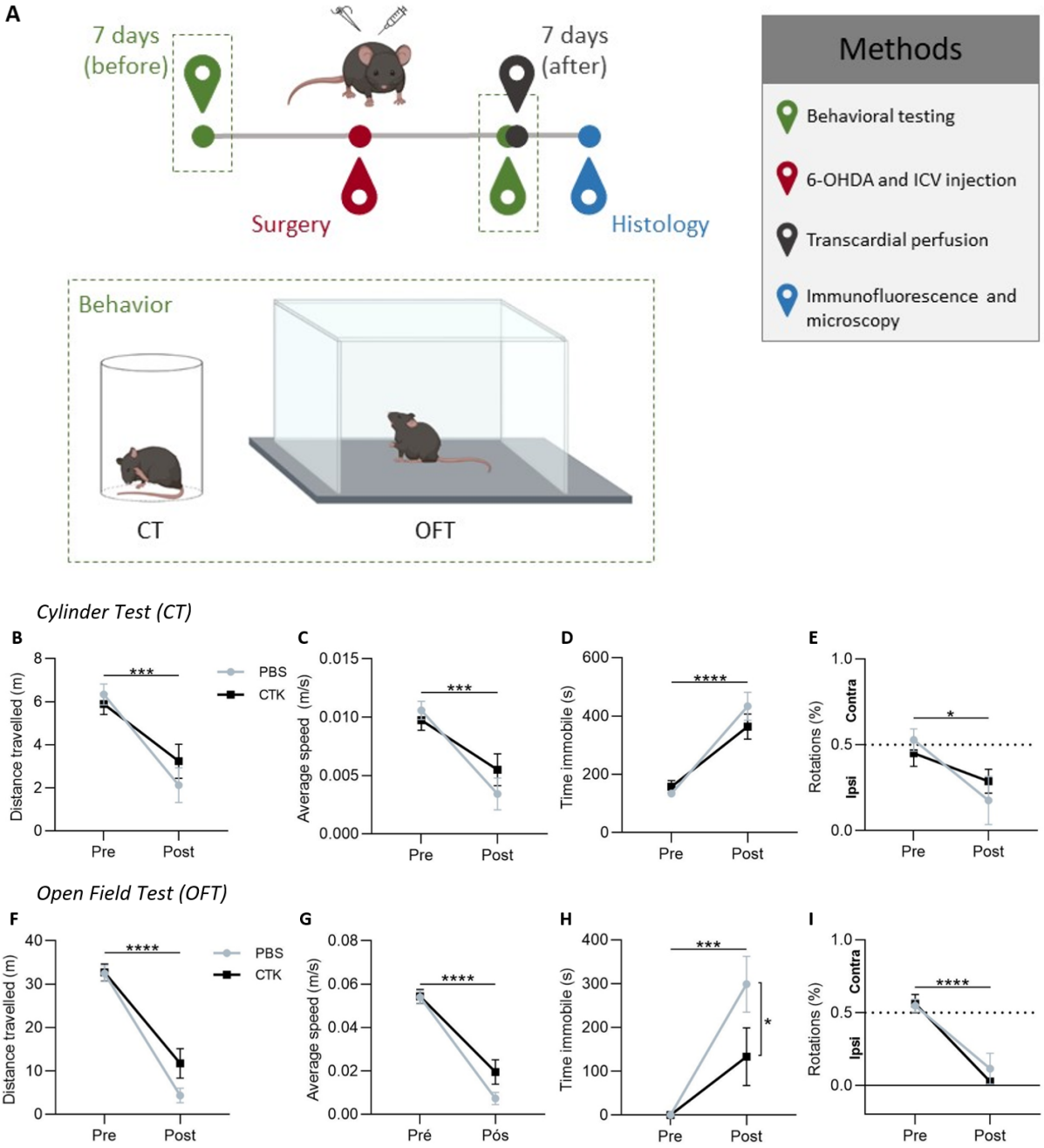

Figure 4. CTK treatment does not improve motor dysfunction in mice with unilateral dopamine depletion. **(A)** Experimental design showing behavioral assessment before and after induction of dopaminergic neurodegeneration (6-OHDA), and ICV injection for treatment with CTK or PBS. **(B, C, D, E)**. Evaluation of motor parameters in the cylinder test (CT), such as distance travelled **(B)**, average speed **(C)**, time immobile **(D)** and rotations **(E)**. **(F, G, H, I)** Evaluation of the same motor parameters, respectively, but in the open field test (OFT). Data represented as mean ± S.E.M. (n = 7 CTK group/ 8 PBS group). ***P < 0.001, **P < 0.01, *P < 0.05.

0.3958; 0.50: -0.00452, 95% CI -0.02269 to 0.01367, $t_{(6)}$ = 0.6071, p = 0.5660; 0.14: -0.00727, 95% CI -0.02581 to 0.01127, $t_{(6)}$ = 0.9598, p = 0.3742; -0.22: -0.01102, 95% CI -0.02923 to 0.007204, $t_{(6)}$ = 1.479, p = 0.1896; 0.86 to -0.22 (average):

-0.0073, 95% CI -0.02661 to 0.01115, $t_{(6)}$ = 1.002, p = 0.3550, Student's *t*-test; **Figure 5E**).

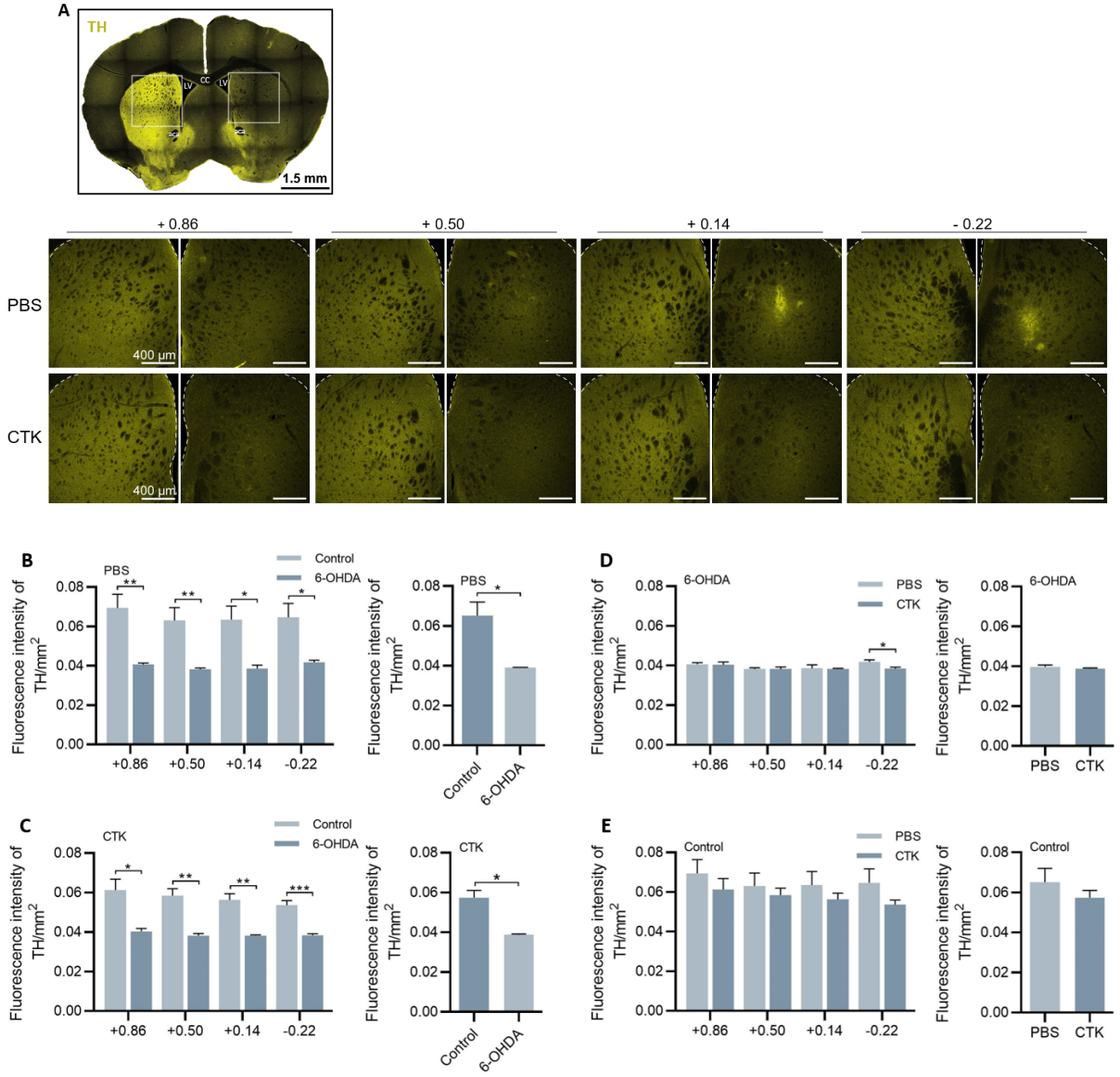

Figure 5. CTK treatment did not alter the dopaminergic neurodegeneration caused by 6-OHDA in the striatum after 7 days. (A) Representative coronal fluorescent images of dopamine-intact (control) or dopamine-depleted (6-OHDA) in the striatal subregions at AP +0.86, +0.50, +0.14 and -0.22, in the group treated with CTK or PBS. Yellow fluorescence on striatum represents TH immunoreactivity. **(B, C)** Quantification of fluorescence intensity of TH in the dopaminergic fibers of the striatum, in the depleted- (6-OHDA) and intact- (control) hemispheres, in the different coordinates and in the general average of these four subregions, in the group that received PBS (ICV) **(B)** and in the group that received treatment (ICV) of CTK **(C). (D, E)** Quantification of fluorescence intensity of TH between the group treated with PBS and CTK, in the different coordinates and in the general average of these four slices, in the ipsilateral hemisphere **(D)** or between the contralateral hemisphere **(E)**. Data represented as mean ± S.E.M. (N = 4/group). ***P < 0.001, **P < 0.01, *P < 0.05. CC: Corpus Callosum. LV: Lateral Ventricle. ACA: Anterior Commissure.

Together, these results suggest that under the process of dopaminergic depletion caused by 6-OHDA, CTK did not reverse the initial alteration of motor behavior, and did not demonstrate effect on the process of neurodegeneration in the striatum.

3.4.4 CTK treatment reduces the formation of glial scar on the anterior subregion of the striatum in the AP axis

As the induction of the dopaminergic neurodegeneration causes microgliosis and astrogliosis, we analyzed the response of these cells under the treatment with ICV injection of CTK or PBS after 7 days (**Figure 6A and Figure 7A**).

To assess the microglia, we measured the fluorescence intensity of $Iba1^+$ on four subregions of the striatum. Interestingly, the group that received PBS ICV infusion showed significant increase in fluorescence intensity on three striatal coordinates (AP +0.50mm, +0.14mm, -0.22mm), when compared with the control hemisphere (0.86: 2.67, 95% CI -10.43 to 5.086, $t_{(4)} = 0.9560$, $p = 0.3932$; 0.50: 26.7, 95% CI -31.55 to -21.85, $t_{(4)} = 15.29$, $p = 0.0001$; 0.14: 32.89, 95% CI -40,84 to -24,95, $t_{(4)} = 11.49$, $p = 0.0003$; -0.22: 34.61, 95% CI -48.83 to -20.39, $t_{(4)} = 6.758$, $p = 0.0025$; 0.86 to -0.22 (average): 24.22, 95% CI -40,82 to -7,617, $t_{(6)} = 3.570$, $p = 0.0118$, Student's *t*-test; **Figure 6B**), while the CTK-treated group exhibited this difference only on the two posterior subregions (AP +0.14mm and -0.22mm) (0.86: 4.19, 95% CI -8.604 to 0.2164, $t_{(4)} = 2.640$, $p = 0.0576$; 0.50: 8.32, 95% CI -21.14 to 4.511, $t_{(4)} = 1.800$, $p = 0.1463$; 0.14: 35.65, 95% CI -59.91 to -11.40, $t_{(4)} = 4.081$, $p = 0.0151$; -0.22: 48.86, 95% CI -64.75 to -33.06, $t_{(4)} = 8.568$, $p = 0.0010$; 0.86 to -0.22 (average): 24.22, 95% CI -48,99 to -0,4585, $t_{(6)} = 2.493$, $p = 0.0470$, Student's *t*-test; **Figure 6C**).

We next compared fluorescence intensity of $Iba1^+$ between the PBS and CTK groups. As observed in the representative microscopy images (**Figure 6A**), on the dopamine-depleted hemisphere, the CTK-treated group showed less fluorescence intensity of microglia cells, on the striatum at the coordinate +0.50mm, compared with PBS-treated group (PBSxCTK: 0.86: 1.52, 95% CI -3.817 to 6.858, $t_{(4)} = 0.7910$, $p = 0.4732$; 0.50: -17.33, 95% CI -27.64 to -7.019, $t_{(4)} = 4.666$, $p = 0.0095$; 0.14: 3.22, 95% CI -21.77 to 28.21, $t_{(4)} = 0.3576$, $p = 0.7387$; -0.22: MedianD 11.61, $p = 0.4000$, Student's *t*-test or Mann-Whitney; **Figure 6D**). The average of the four striatal subregions did not show a significant difference (PBSxCTK: 0.86 to -0.22 (average): 0.29, 95% CI -28.96 to 29.55, $t_{(6)} = 0.02493$, $p = 0.9809$, Student's *t*-test; **Figure 6D**).

No difference between groups was observed on the control hemisphere (PBSxCTK: 0.86: -1.85, 95% CI -9.924 to 6.237, $t_{(4)}$ =0.6335, p = 0.5608; 0.50: 1.05, 95% CI -7.979 to 10.09, $t_{(4)}$ = 0.3251, p = 0.7614; 0.14: 0.46, 95% CI -4.741 to 5.653, $t_{(4)}$ = 0.2438, p = 0.8194; -0.22: -0.51, 95% CI -7.736 to 6.716, $t_{(4)}$ = 0.1959, p = 0.8542; 0.86 to -0.22 (average): -0.21, 95% CI -3.166 to 2.746, $t_{(6)}$ = 0.1737, p = 0.8678, Student's *t*-test; **Figure 6E**).

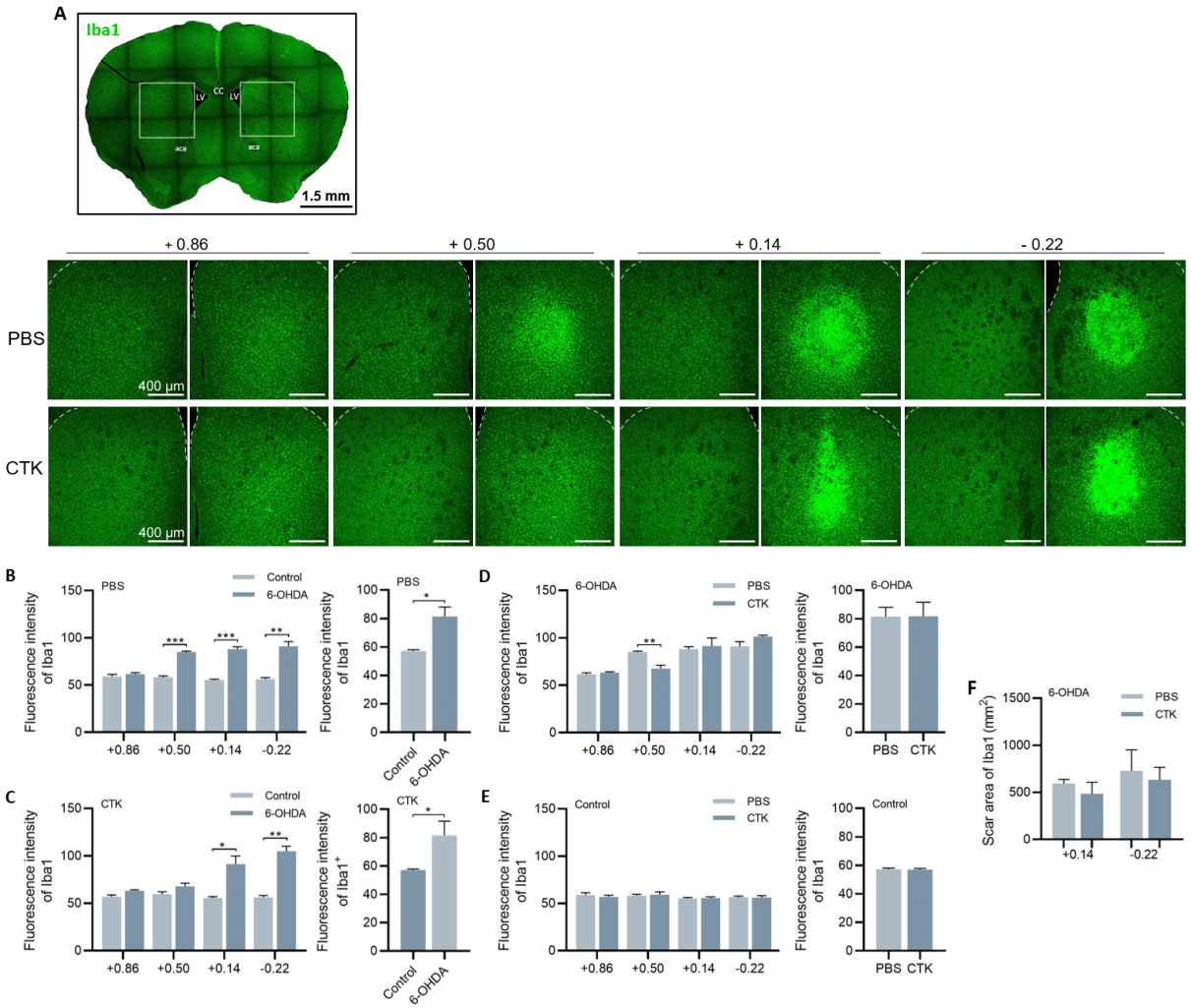

Figure 6. CTK treatment reduces the formation of microglial scar on the anterior subregion of the striatum in the AP axis. (A) Representative coronal fluorescent images of Iba1$^+$ of the groups treated with CTK or PBS. The green fluorescent concentrate of Iba1$^+$ corresponds to the microglial scar. **(B, C)** Quantification of fluorescence intensity of Iba1$^+$ in the dopamine-depleted (6-OHDA) and intact (control) hemispheres, in the different striatal subregions and in the general average of these four slices, of the group that received ICV injection of PBS **(B)** and of the group that received CTK treatment (ICV) **(C). (D,E)** Quantification of fluorescence intensity of Iba1$^+$ between the groups treated with PBS or CTK, in the different coordinates and in the general average of these four slices, in the 6-OHDA injected hemisphere **(D)** or between the control hemisphere **(E)**. **(F)** Scar area formed by Iba1$^+$. Data represented as mean ± S.E.M. (n = 4/group). ****P < 0.0001, ***P < 0.001, **P < 0.01. CC: Corpus Callosum. LV: Lateral Ventricle. ACA: Anterior Commissure.

The group treated with CTK started to present a scar on AP coordinate +0.14mm, so we measured the area only in the last two coordinates. No significant difference was found between the groups (PBSxCTK: 0.14: -109.6, 95% CI -480.0 to

260.9, $t_{(4)}$ = 0.8211, p = 0.4577; -0.22: -93.7, 95% CI -818.8 to 631.3, $t_{(4)}$ = 0.3589, p = 0.7378, Student's *t*-test; **Figure 6F**). These findings suggest that CTK treatment reduced the anteroposterior area of microglia scar formation on this neuroinflammation caused by dopaminergic neurodegeneration.

We also assessed astrogliosis under CTK treatment. With the astrocytes receding from the center to the periphery of the scar, we observed, in the group receiving CTK, the absence of $GFAP^+$ in the core lesion only in AP -0.22mm, but in the group treated with PBS it was possible to observe the lack of these cells starting at AP +0.50mm. This absence was clearly observed in AP +0.14mm and -0.22mm (**Figure 7A**). Fluorescence intensity of the astrocytes was higher in the hemisphere injected with 6-OHDA when compared to the control side, in all striatal subregions or in the average of them, in both groups (PBS: 0.86: 17.75, 95% CI -23.00 to -12.51, $t_{(4)}$ = 9.398, p = 0.0007; 0.50: 12.78, 95% CI -22.11 to -3.458, $t_{(4)}$ = 3.806, p = 0.0190; 0.14: 12.99, 95% CI -19.61 to -6.371, $t_{(4)}$ = 5.449, p = 0.0055; -0.22: 15.64, 95% CI -28.15 to -3.128, $t_{(4)}$ =3.471, p = 0.0256; 0.86 to -0.22 (average): 14.79, 95% CI -18.08 to -11.50, $t_{(6)}$ = 11.00, p = 0.0001; **Figure 7B**; CTK: 0.86: 14.1, 95% CI -20.69 to -7.507, $t_{(4)}$ = 5.938, p = 0.0040; 0.50: 18.13, 95% CI -27.24 to -9.028, $t_{(4)}$ = 5.529, p = 0.0052; 0.14: 19.63, 95% CI -27.70 to -11.57, $t_{(4)}$ = 6.760, p = 0.0025; -0.22: 24.66, 95% CI -48.06 to -1.258, $t_{(4)}$ = 2.926, p = 0.0430; 0.86 to -0.22 (average): 19.13, 95% CI -23.87 to -14.39, $t_{(6)}$ = 9.874, p = 0.0001, Student's *t*-test; **Figure 7C**).

The absence of cells in the center, with their migration to form the penumbra zone, was not enough to cause a significant decrease in fluorescence, on the region with astrogliosis, between the treatment groups (PBSxCTK: 0.86: -3.23, 95% CI -11.32 to 4.862, $t_{(4)}$ =1.108, p = 0.3300; 0.50: 6.27, 95% CI -6.177 to 18.70, $t_{(4)}$ = 1.398, p = 0.2347; 0.14: 6.36, 95% CI -3.765 to 16.49, $t_{(4)}$ = 1.744, p = 0.1561; -0.22: 8.63, 95% CI -17.73 to 35.00, $t_{(4)}$ = 0.9092, p = 0.4147; 0.86 to -0.22 (average): 4.51, 95% CI -1.131 to 10.15, $t_{(6)}$ = 1.956, p = 0.0982, Student's *t*-test; **Figure 7D**). Since the control side did not present astrocyte response, no difference in the fluorescence intensity of $GFAP^+$ was found (PBSxCTK: 0.86: 0.42, 95% CI -1.922 to 2.777, $t_{(4)}$ =0.5054, p = 0.6399; 0.50: 0.92, 95% CI -2.967 to 4.792, $t_{(4)}$ = 0.6532, p = 0.5493; 0.14: -0.28, 95% CI -2.783 to 2.221, $t_{(4)}$ = 0.3119, p = 0.7707; -0.22: -0.39, 95% CI -3.390 to 2.616, $t_{(4)}$ = 0.3579, p = 0.7385; 0.86 to -0.22 (average): 0.17, 95% CI -1.065 to 1.401, $t_{(6)}$ = 0.3335, p = 0.7501, Student's *t*-test; **Figure 7E**). The central

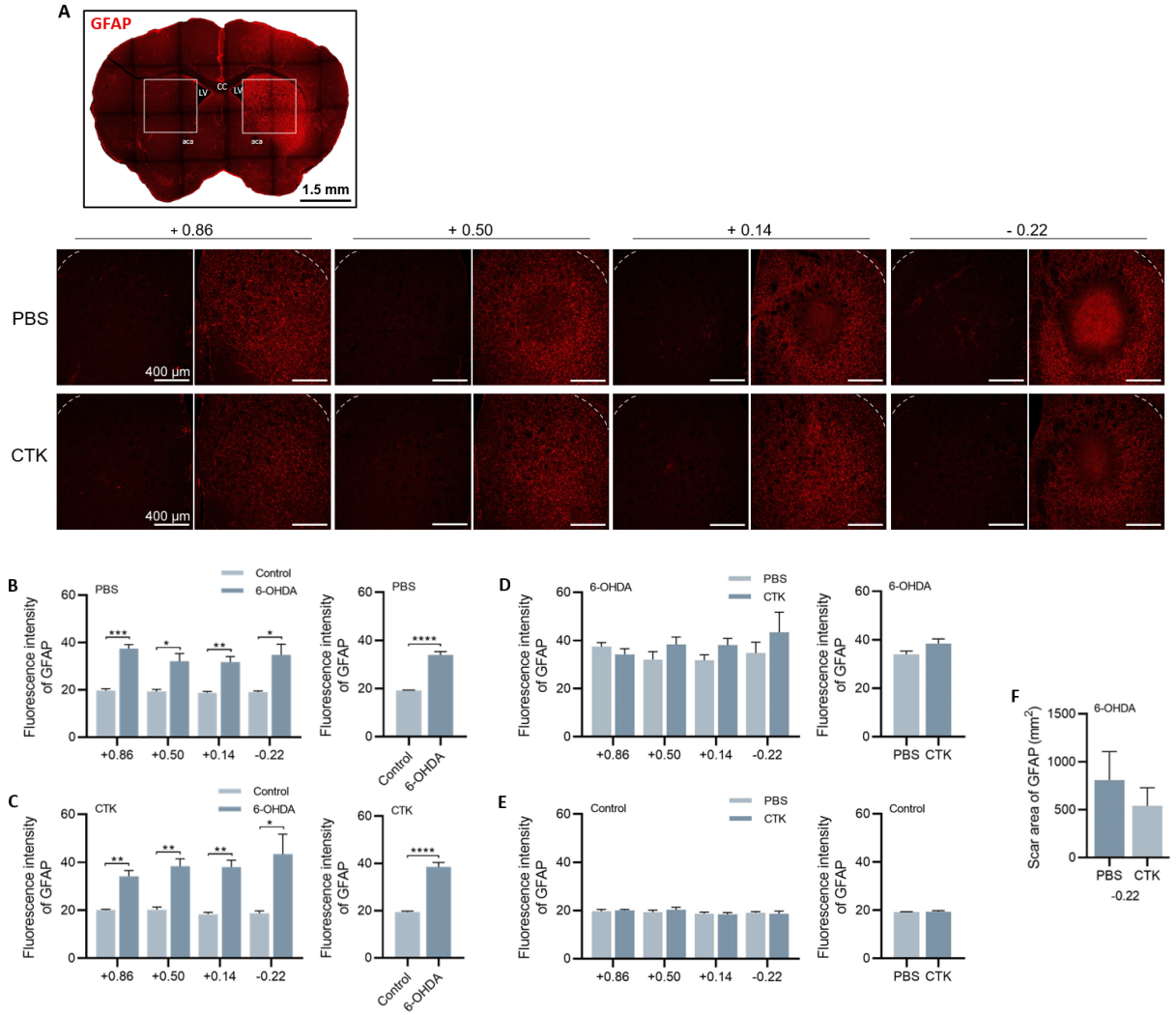

Figure 7. CTK treatment reduces the formation of astrocytic scar on the anterior subregion of the striatum in the AP axis. (A) Representative coronal fluorescent images of GFAP⁺ of the groups treated with CTK or PBS. The circular area in the ipsilateral hemisphere represents the site of astrocytic retreat from the center to the periphery of the scar. **(B, C)** Quantification of fluorescence intensity of GFAP⁺ in the dopamine-depleted (6-OHDA) and in the control hemispheres, in the different AP striatal subregions and in the general average of the four slices, in the group that received PBS ICV infusion **(B)** and in the group that received CTK treatment (ICV) **(C). (D, E)** Quantification of fluorescence intensity of GFAP⁺ between the groups treated with PBS or CTK, in the different coordinates and in the general average of the four slices, in the ipsilateral hemisphere **(D)** or between the contralateral hemisphere **(E)**. **(F)** Scar area formed by GFAP⁺ retreat. Data represented as mean ± S.E.M. (n = 4/group). ***P < 0.001, **P < 0.01, *P < 0.05. CC: Corpus Callosum. LV: Lateral Ventricle. ACA: Anterior Commissure.

area where the astrocytes evacuated did not present a difference between the groups with distinct treatments on AP -0.22mm (PBSxCTK: -0.22: -269.6, 95% CI -1249 to 709.7, $t_{(4)}$ = 0.7644, p = 0.4872, Student's *t*-test; **Figure 7F**). Therefore, CTK exhibited a reducing effect on the formation of the scar in the anterior regions of the site with astrogliosis, following what was observed with the microglia.

In short, the treatment with CTK 01512-2, the recombinant version of Phα1β, was able to reduce the formation of microglial and astrocytic scar in anterior subregions of the striatum in the AP axis.

3.5 DISCUSSION

The CNS immune system plays crucial activities. The inflammatory process is important, however it can cause damage. Microglia is essential on lesion debridement, elimination of pathogens, release of neurotrophic factor and regulation of the microenvironment (ZIV et al., 2006; CHOUDHURY et al., 2011; PISANU et al., 2014), but under intense inflammatory process, as is seen in chronic neurodegenerative diseases, it is related to neuronal death, by excessive production of proinflammatory cytokines, and nitric oxide (NO), as well as promoting the phagocytosis of premature neurons under degeneration (MARINOVA-MUTAFCHIEVA et al., 2009; DE LELLA et al., 2010; QIAN et al., 2010; LEVESQUE et al., 2010; LEUNG et al., 2011). Reactive astrocytes in the inflammatory process site are essential to limit the generalized damage, containing spread of inflammatory cells or infectious agents. They also regulate oxidative stress and are involved in the blood-brain barrier (BBB) repair (CHEN et al., 2001; FAULKNER et al., 2004; VARGAS et al., 2008; CHEN et al., 2009; VOSKUHL et al., 2009). However, it was shown that excessive immune response, along with long lasting compact glial scar, inhibits neuronal regeneration, generates excessive production of proinflammatory cytokines and ROS, and could compromise BBB function (SILVER et al., 2004; HAMBY et al., 2006; ARGAW et al., 2009; BRAMBILLA et al., 2009; WANNER et al., 2013). Some studies have suggested that the possibility to adjust the intensity of the inflammatory response could be beneficial without the loss of the positive actions of glial reactivity (SCHWART et al., 2006; GLEZER et al., 2007; GARG et al., 2008; SOFRONIEW and VINTERS, 2010; YANG et al., 2020).

In this study, we demonstrated that in a PD mouse model induced by 6-OHDA, the neurodegeneration of the dopaminergic striatal fibers causes a microglia and astrocyte activation, and under the conditions presented, we provided a characterization, through the microscopic perspective, of microglia and astrocytes response along 6 months.

In the quantitative analysis, microglia started to show a significant response 24 hours after the 6-OHDA injection, with intensification of this process after 3 days (**Figure 2B-F**). When we compared the response in the different time points (intergroups) on the same striatal subregions, it is notable that the hemisphere with induction of neurodegeneration demonstrates a higher quantification of microglia at 24 hours and 3 days, when compared with the other time points (**Figure 2G-K**). In the 3- and 6- month groups we observed a reduction of the number of cells that was, in some points, lower than the observed at 3 hours (**Supplementary tables 1**). This decline suggests a reduction of the inflammatory process, which could be associate with the fact that, in this rodent model, spontaneous recovery of the dopaminergic fibers has been observed after 6 months of lesion, reinforcing this model as “acute”, with restrictions for long-term studies (BLANCHARD et al., 1995; STANIC et al., 2003). The scar formation is usually analysed in a qualitative and observative way, by microscopy images. Here, since it was not possible to quantify $Iba1^+$ cells, because of the core formation, we measured the fluorescence and the area of the scar presented in some subregions in the 3- and 7-day groups (**Figure 2N-Q**). This type of assessment has some limitations, such as the fact that the measurements only take into account the ML and DV axes of the mouse brain.

The astrocytes response was identified next. The GFAP protein, marked to identify these cells, is in high expression when the cell is reactive. Here, we started to observe immunoreactive $GFAP^+$ cells 3 days after lesion (**Figure 3A**). Interestingly, at 24 hours it was possible to identify an increase in the background of the side of 6-OHDA injection, suggesting that astrocytes are already becoming reactive, which was not seen at 3 hours (**Figure 3B-C**). The identification of $GFAP^+$ astrocytes, when reactive, was seen distributed on the StDM. At 3 days, we observed it evacuating from the center to form the penumbra zone in some subregions, which is evident after more time, since we could identify a better delimitation of the astrocytic scar and the hypertrophic morphology at the scar periphery at 7 days. The evaluation after 3 and 6 months showed similarities with the microglial scar, since at these time points the identification of $GFAP^+$ cell is limited to the posterior region of the AP axis, and at the place that was the core in the mature lesion (**Figure 3H-N** and **Supplementary tables 4**). The higher intensity of fluorescence after 7 days with the clear visualization of the astrocytes, in the expected conformation and distribution, put this

time point as the most reactive in this analysis. We found the same limitations to quantify parameters of the astrocytes scar, as seen in the microglia analysis.

The hemisphere injected with PBS showed, on microscopy images, a reaction in the region of the needle-tract where the sterile control injection was made (**Figure 2A** and **3A**), and this is expected since a mechanical lesion and pressure imbalance from solution infusion occurs (WALSH et al., 2011, LEE et al., 2018; PRÁ et al., 2019). The microglia and astrocyte response was not able to cause a scar formation, and when compared with the side that received 6-OHDA, the glial reaction was discrete and limited.

The reduction of dopaminergic fiber shown here, by the decrease in TH fluorescence intensity between the hemispheres, was presented similarly by the groups treated with CTK and PBS (**Figure 5A-C**). Some studies noticed that the precise identification of the preference for the use of the ipsilateral forelimb in vertical exploration occurred when the unilateral neurodegeneration on striatal fibers was approximately 60-70%, so usually experiments accessing this parameter are performed around 3-4 weeks after surgery (BLANDINI et al., 2007; MAGNO et al., 2019a, ANTUNES et al., 2020). At this point, the lesion is more intense and the animals already left the recovery period (7 days) of the surgical procedure. Here, we showed that even after only 7 days, the animals presented some of the expected physical alterations, as preference of rotation for the ipsilateral side (**Figure 4A-I**). A behavioral analysis after more time would insure a higher level of dopamine-depletion and could give a better identification of the changes on motor behavior, as well as ensure that the reduction in distance traveled, average speed, and the increase in immobile time were due to motor changes caused by the dysfunction of the nigrostriatal pathway, and not due to the the exhaustion caused by the surgery process, since at the time point we assessed, the animals were leaving the recovery phase.

In addition to the analgesic potential of Phα1β and its recombinant version CTK 01512-2, some studies have recently drawn attention to their anti-inflammatory potential. Silva and colleagues (2018) demonstrated the action of CTK in a mouse model of MS, by reduction of microglia and astrocyte reaction, decrease of pro-inflammatory cytokines, with prevention on axonal loss and improving coordination, cognition and the clinical course of MS. The effect of Phα1β on glial cells was capable of remodeling the reactive microglia morphology and astrocytic

proliferation in spinal cord gliosis following peripheral inflammation (TENZA-FERRER et al., 2019). Here, we showed that CTK was able to reduce the scar formation caused by reactive microglia and astrocytes on anterior subregions of the striatum under dopaminergic neurodegeneration. This inflammatory reaction is considered severe, since we identified a compact glial scar formation (**Figure 6** and **7**).

We hypothesized that the reduction of the glial response could possibly influenciate the dopaminergic neurodegeneration. Studies of interventions on the microglia response, decreasing its activation, have suggested that this can reduce dopaminergic cell death in animal models (ZHANG et al., 2006, CASAREJOS et al., 2006; MCCOY et al., 2006; MOUNT et al., 2007), but in this study we did not observe a reduction of the neurodegeneration of the dopaminergic striatal fibers (**Figure 5D-E**).

The evaluation of a higher dose of CTK could demonstrate an intense anti-inflammatory effect on astrocytes and microglia, and this did not represent a risk of intoxication, since other studies used higher doses of Phα1β or CTK, and started to identify discrete adverse effects at doses of 100 pmol/site (RIGO et al., 2013a; RIGO et al., 2017; SILVA et al., 2018). Furthermore, here we executed the CTK injection immediately after induction of dopaminergic neurodegeneration. Performing CTK infusion before the neurodegenerative process would show us if an effect of neuroprotection would be observed. Besides that, if it was infused after the dopaminergic neurodegeneration started it would indicate how microglia and astrocytes would respond. This also opens questions if the treatment with CTK did not show effect on other points of the nigrostriatal pathway, and how the cell bodies in the SNc react to the gliosis process, in the condition presented, and the progress of the neurodegeneration in other time points.

In conclusion, our findings demonstrated an immunofluorescence characterization of microglia and astrocyte response to 6-OHDA Parkinson's mouse model in 6 time points. We also showed that CTK-01512-2 was able to reduce glial scar formation at the point with higher inflammatory cells reaction. Our study therefore suggests that other doses of the recombinant toxin, different routes of administration and the moment of its application are necessary to better understand this anti-inflammatory effect.

REFERENCES

References are at the end of this dissertation.

4.0 CONCLUSION AND FUTURE PERSPECTIVES

The 6-OHDA PD mouse model used here showed astrocytes and microglia reactivity with scar formation, and the 7 day-group was the higher inflammation time point.

An evaluation after 7 days could give a scenario of how microgliosis and astrogliosis advance before the decline of the reactivite at 3 months.

A verification of the dopaminergic neurodegeneration with the glia response, on the timeline analyses, would allow a correlation between inflammation and neurodegeneration of the nigrostriatal pathway.

The use of a chronic neurodegeneration mouse model would allow us to verify a greater similarity to that seen in the PD patients.

Treatment with CTK 01512-2 reduced the scar formation on the AP axis, showing an anti-inflammatory effect on severe glial reactivity.

A different dose could show a more intense effect in the reactive cells.

An infusion before the induction of neurodegeneration could allow the verification of neuroprotective effects.

The treatment with CTK 01512-2 in a time point after the beginning of the neurodegeneration could give us a prospective use of this toxin similar to the clinical treatment.

A different method of administration, less invasive, as intravenous injection, would represent a more accessible alternative of treatment.

The assessment of the effects of a chronic treatment with CTK intravenously would allow us to verify its action over time.

5.0 REFERENCES

Abbott, N. J., Rönnbäck, L. & Hansson, E. Astrocyte-endothelial interactions at the blood-brain barrier. *Nature Reviews Neuroscience* vol. 7 (2006).

Agostini, R. M. *et al.* Phoneutria spider toxins block ischemia-induced glutamate release and neuronal death of cell layers of the retina. *Retina* **31**, (2011).

Akiyama, H. *et al.* Inflammation and Alzheimer's disease. *Neurobiology of Aging* vol. 21 (2000).

Almeida, A. P. *et al.* Antiarrhythmogenic effects of a neurotoxin from the spider Phoneutria nigriventer. *Toxicon* **57**, (2011).

Antunes, F. T. T. *et al.* Recombinant peptide derived from the venom the Phoneutria nigriventer spider relieves nociception by nerve deafferentation. *Neuropeptides* **79**, (2020).

Argaw, A. T., Gurfein, B. T., Zhang, Y., Zameer, A. & John, G. R. VEGF-mediated disruption of endothelial CLN-5 promotes blood-brain barrier breakdown. *Proc. Natl. Acad. Sci. U. S. A.* **106**, (2009).

Arújo, D. A. M., Cordeiro, M. N., Diniz, C. R. & Beirão, P. S. L. Effects of a toxic fraction, PhTx2, from the spider Phoneutria nikriventer on the sodium current. *Naunyn. Schmiedebergs. Arch. Pharmacol.* **347**, (1993).

Blanchard, V. et al. Long‐Term Induction of Tyrosine Hydroxylase Expression: Compensatory Response to Partial Degeneration of the Dopaminergic Nigrostriatal System in the Rat Brain. J. Neurochem. **64**, (1995).

Blandini, F., Levandis, G., Bazzini, E., Nappi, G. & Armentero, M. T. Time-course of nigrostriatal damage, basal ganglia metabolic changes and behavioural alterations following intrastriatal injection of 6-hydroxydopamine in the rat: New clues from an old model. Eur. J. Neurosci. **25**, (2007).

Block, M. L., Zecca, L. & Hong, J. S. Microglia-mediated neurotoxicity: Uncovering the molecular mechanisms. *Nature Reviews Neuroscience* vol. 8 (2007).

Braak, H., Sastre, M. & Del Tredici, K. Development of α-synuclein immunoreactive astrocytes in the forebrain parallels stages of intraneuronal pathology in sporadic Parkinson's disease. *Acta Neuropathol.* **114**, (2007).

Brambilla, R. *et al.* Transgenic Inhibition of Astroglial NF-κB Improves Functional Outcome in Experimental Autoimmune Encephalomyelitis by Suppressing Chronic Central Nervous System Inflammation. *J. Immunol.* **182**, (2009).

Bucaretchi, F. *et al.* Systemic envenomation caused by the wandering spider Phoneutria nigriventer, with quantification of circulating venom. *Clin. Toxicol.* **46**, (2008).

Bush, T. G. *et al.* Leukocyte infiltration, neuronal degeneration, and neurite outgrowth after ablation of scar-forming, reactive astrocytes in adult transgenic mice. *Neuron* **23**, (1999).

Casarejos, M. J. et al. Susceptibility to rotenone is increased in neurons from parkin null mice and is reduced by minocycline. J. Neurochem. **97**, (2006).

Chen, P. C. *et al.* Nrf2-mediated neuroprotection in the MPTP mouse model of Parkinson's disease: Critical role for the astrocyte. *Proc. Natl. Acad. Sci. U. S. A.* **106**, (2009).

Chen, Y. *et al.* Astrocytes protect neurons from nitric oxide toxicity by a glutathione-dependent mechanism. *J. Neurochem.* **77**, (2001).

Choudhury, M. E. *et al.* A cytokine mixture of GM-CSF and IL-3 that induces a neuroprotective phenotype of microglia leading to amelioration of (6-OHDA)-induced Parkinsonism of rats. *Brain Behav.* **1**, (2011).

Cicchetti, F. *et al.* Neuroinflammation of the nigrostriatal pathway during progressive 6-OHDA dopamine degeneration in rats monitored by immunohistochemistry and PET imaging. *Eur. J. Neurosci.* **15**, (2002).

Damier, P., Hirsch, E. C., Zhang, P., Agid, Y. & Javoy-Agid, F. Glutathione peroxidase, glial cells and Parkinson's disease. *Neuroscience* **52**, (1993).

Davalos, D. *et al.* ATP mediates rapid microglial response to local brain injury in vivo. *Nat. Neurosci.* **8**, (2005).

De Lella Ezcurra, A. L., Chertoff, M., Ferrari, C., Graciarena, M. & Pitossi, F. Chronic expression of low levels of tumor necrosis factor-α in the substantia nigra elicits progressive neurodegeneration, delayed motor symptoms and microglia/macrophage activation. *Neurobiol. Dis.* **37**, (2010).

de Lima, M. E. *et al.* Phoneutria nigriventer Venom and Toxins: A Review. in *Spider Venoms* (2015). doi:10.1007/978-94-007-6646-4_6-1.

Ellis, S., Lin, E. J. & Tartar, D. Immunology of Wound Healing. *Current Dermatology Reports* vol. 7 (2018).

Emerich, B. L. *et al.* δ-ctenitoxin-pn1a, a peptide from phoneutria nigriventer spider venom, shows antinociceptive effect involving opioid and cannabinoid systems, in rats. *Toxins (Basel).* **8**, (2016).

Faulkner, J. R. *et al.* Reactive Astrocytes Protect Tissue and Preserve Function after Spinal Cord Injury. *J. Neurosci.* **24**, (2004).

Garg, S. K., Banerjee, R. & Kipnis, J. Neuroprotective Immunity: T Cell-Derived Glutamate Endows Astrocytes with a Neuroprotective Phenotype. *J. Immunol.* **180**, (2008).

Garver, D. L., Cedarbaum, J. & Maas, J. W. Blood-brain barrier to 6-hydroxydopamine: Uptake by heart and brain. *Life Sci.* **17**, (1975).

Glass, C. K., Saijo, K., Winner, B., Marchetto, M. C. & Gage, F. H. Mechanisms Underlying Inflammation in Neurodegeneration. *Cell* vol. 140 (2010).

Glinka, Y. Y. & Youdim, M. B. H. Inhibition of mitochondrial complexes I and IV by 6-hydroxydopamine. *Eur. J. Pharmacol. Environ. Toxicol.* **292**, (1995).

Gomez, M. V, Kalapothakis, E., Guatimosim, C. & Prado, M. A. M. Phoneutria nigriventer venom: A cocktail of toxins that affect ion channels. *Cellular and Molecular Neurobiology* vol. 22 (2002).

Göritz, C. *et al.* A pericyte origin of spinal cord scar tissue. *Science (80-.).* **333**, (2011).

Grishin, E. Polypeptide neurotoxins from spider venoms. *European Journal of Biochemistry* vol. 264 (1999).

Halassa, M. M., Fellin, T. & Haydon, P. G. The tripartite synapse: roles for gliotransmission in health and disease. *Trends Mol. Med.* **13**, (2007).

Hamby, M. E., Hewett, J. A. & Hewett, S. J. TGF-β1 potentiates astrocytic nitric oxide production by expanding the population of astrocytes that express NOS-2. *Glia* **54**, (2006).

Herrmann, J. E. *et al.* STAT3 is a critical regulator of astrogliosis and scar formation after spinal cord injury. *J. Neurosci.* **28**, (2008).

Horn, K. P., Busch, S. A., Hawthorne, A. L., Van Rooijen, N. & Silver, J. Another barrier to regeneration in the CNS: Activated macrophages induce extensive retraction of dystrophic axons through direct physical interactions. *J. Neurosci.* **28**, (2008).

Kim, S. U. & De Vellis, J. Microglia in health and disease. *Journal of Neuroscience Research* vol. 81 (2005).

Kirik, D., Rosenblad, C. & Björklund, A. Characterization of behavioral and neurodegenerative changes following partial lesions of the nigrostriatal dopamine system induced by intrastriatal 6-hydroxydopamine in the rat. *Exp. Neurol.* **152**, (1998).

Kostrzewa, R. M. & Jacobowitz, D. M. Pharmacological actions of 6 hydroxydopamine. *Pharmacological Reviews* vol. 26 (1974).

Lastres-Becker, I., Molina-Holgado, F., Ramos, J. A., Mechoulam, R. & Fernández-Ruiz, J. Cannabinoids provide neuroprotection against 6-hydroxydopamine toxicity in vivo and in vitro: Relevance to Parkinson's disease. *Neurobiol. Dis.* **19**, (2005).

Leung, Y. M. P2X7 receptor as a double-edged sword: Neurotrophic and neurotoxic effects. *BioMedicine (Netherlands)* vol. 1 (2011).

Levesque, S. *et al.* Reactive microgliosis: Extracellular-calpain and microglia-mediated dopaminergic neurotoxicity. *Brain* **133**, (2010).

Lucas, S. Spiders in Brazil. *Toxicon* vol. 26 (1988).

Magno, L. A. V. *et al.* Optogenetic stimulation of the M2 cortex reverts motor dysfunction in a mouse model of Parkinson's disease. *J. Neurosci.* **39**, (2019a).

Magno, L. A., Collodetti, M., Tenza-Ferrer, H. & Romano-Silva, M. Cylinder Test to Assess Sensory-Motor Function in a Mouse Model of Parkinson's Disease. *BIO-PROTOCOL* **9**, (2019b).

Magno, L. A. V. *et al.* Contribution of neuronal calcium sensor 1 (Ncs-1) to anxiolytic-like and social behavior mediated by valproate and Gsk3 inhibition. *Sci. Rep.* **10**, (2020).

Marin, C., Aguilar, E., Mengod, G., Cortés, R. & Obeso, J. A. Concomitant short- and long-duration response to levodopa in the 6-OHDA-lesioned rat: A behavioural and molecular study. *Eur. J. Neurosci.* **25**, (2007).

Marinova-Mutafchieva, L. *et al.* Relationship between microglial activation and dopaminergic neuronal loss in the substantia nigra: A time course study in a 6-hydroxydopamine model of Parkinson's disease. *J. Neurochem.* **110**, (2009).

McCoy, M. K. *et al.* Blocking soluble tumor necrosis factor signaling with dominant-negative tumor necrosis factor inhibitor attenuates loss of dopaminergic neurons in models of Parkinson's disease. *J. Neurosci.* **26**, (2006).

McGeer, P. L. & McGeer, E. G. Inflammatory processes in amyotrophic lateral sclerosis. *Muscle and Nerve* vol. 26 (2002).

Meletis, K. *et al.* Spinal cord injury reveals multilineage differentiation of ependymal cells. *PLoS Biol.* **6**, (2008).

Mount, M. P. et al. Involvement of interferon-γ in microglial-mediated loss of dopaminergic neurons. J. Neurosci. **27**, (2007).

Noelker, C. *et al.* The flavanoide caffeic acid phenethyl ester blocks 6-hydroxydopamine- induced neurotoxicity. *Neurosci. Lett.* **383**, (2005).

Parra, I., Martínez, I., Ramírez-García, G., Tizabi, Y. & Mendieta, L. Differential Effects of LPS and 6-OHDA on Microglia's Morphology in Rats: Implications for Inflammatory Model of Parkinson's Disease. *Neurotox. Res.* **37**, (2020).

Pinheiro, A. C. D. N. *et al.* Phoneutria spider toxins block ischemia-induced glutamate release, neuronal death, and loss of neurotransmission in hippocampus. *Hippocampus* **19**, (2009).

Pisanu, A. *et al.* Dynamic changes in pro-and anti-inflammatory cytokines in microglia after PPAR-γ agonist neuroprotective treatment in the MPTPp mouse model of progressive Parkinson's disease. *Neurobiol. Dis.* **71**, (2014).

Qian, L., Flood, P. M. & Hong, J. S. Neuroinflammation is a key player in Parkinson's disease and a prime target for therapy. *Journal of Neural Transmission* vol. 117 (2010).

Rezende, L., Cordeiro, M. N., Oliveira, E. B. & Diniz, C. R. Isolation of neurotoxic peptides from the venom of the 'armed' spider Phoneutria nigriventer. *Toxicon* **29**, (1991).

Rigo, F. K. *et al.* Effect of ω-conotoxin MVIIA and Phα1β on paclitaxel-induced acute and chronic pain. *Pharmacol. Biochem. Behav.* **114**–**115**, (2013a).

Rigo, F. K. *et al.* Spider peptide Phα1β induces analgesic effect in a model of cancer pain. *Cancer Sci.* **104**, (2013b).

Rigo, F. K. *et al.* The spider toxin Phα1β recombinant possesses strong analgesic activity. *Toxicon* **133**, 145–152 (2017).

Rosa, F. *et al.* Phα1β, a peptide from the venom of the spider phoneutria nigriventer shows antinociceptive effects after continuous infusion in a neuropathic pain model in rats. *Anesth. Analg.* **119**, (2014).

Schneider, C. A., Rasband, W. S. & Eliceiri, K. W. NIH Image to ImageJ: 25 years of image analysis. *Nature Methods* vol. 9 (2012).

Schwartz, M., Butovsky, O. & Kipnis, J. Does inflammation in an autoimmune disease differ from inflammation in neurodegenerative diseases? Possible implications for therapy. *Journal of Neuroimmune Pharmacology* vol. 1 (2006).

Segura-Aguilar, J. & Kostrzewa, R. M. Neurotoxin Mechanisms and Processes Relevant to Parkinson's Disease: An Update. *Neurotox. Res.* **27**, (2015).

Silva, R. B. M. *et al.* Beneficial Effects of the Calcium Channel Blocker CTK 01512-2 in a Mouse Model of Multiple Sclerosis. *Mol. Neurobiol.* **55**, (2018).

Silva, R. B. M. *et al.* Spinal blockage of P/Q-or N-type voltage-gated calcium channels modulates functional and symptomatic changes related to haemorrhagic cystitis in mice. *Br. J. Pharmacol.* **172**, (2015).

Sochocka, M., Diniz, B. S. & Leszek, J. Inflammatory Response in the CNS: Friend or Foe? *Molecular Neurobiology* vol. 54 (2017).

Soderblom, C. *et al.* Perivascular fibroblasts form the fibrotic scar after contusive spinal cord injury. *J. Neurosci.* **33**, (2013).

Sofroniew, M. V. & Vinters, H. V. Astrocytes: Biology and pathology. *Acta Neuropathologica* vol. 119 (2010).

Sofroniew, M. V. Astrocyte barriers to neurotoxic inflammation. *Nature Reviews Neuroscience* vol. 16 (2015).

Sofroniew, M. V. Molecular dissection of reactive astrogliosis and glial scar formation. *Trends in Neurosciences* vol. 32 (2009).

Souza, A. H. *et al.* Analgesic effect in rodents of native and recombinant Phα1β toxin, a high-voltage-activated calcium channel blocker isolated from armed spider venom. *Pain* **140**, (2008).

Stanic, D., Finkelstein, D. I., Bourke, D. W., Drago, J. & Horne, M. K. Timecourse of striatal re-innervation following lesions of dopaminergic SNpc neurons of the rat. Eur. J. Neurosci. **18**, (2003).

Sueur, L., Kalapothakis, E. & da Cruz-Höfling, M. A. Breakdown of the blood-brain barrier and neuropathological changes induced by Phoneutria nigriventer spider venom. *Acta Neuropathologica* vol. 105 (2003).

Tenza-Ferrer, H., Magno, L. A. V., Romano-Silva, M. A., da Silva, J. F. & Gomez, M. V. Phα1β spider toxin reverses glial structural plasticity upon peripheral inflammation. *Front. Cell. Neurosci.* **13**, 1–16 (2019).

Tonello, R. *et al.* Action of phα1β, a peptide from the venom of the spider phoneutria nigriventer, on the analgesic and adverse effects caused by morphine in mice. *J. Pain* **15**, (2014).

Tonello, R. *et al.* Phalpha1beta acts as a TRPA1 antagonist with antinociceptive effects in mice. *Br. J. Pharmacol.* (2016).

Tonello, R. *et al.* The peptide Phα1β, from spider venom, acts as a TRPA1 channel antagonist with antinociceptive effects in mice. *Br. J. Pharmacol.* **174**, (2017).

Ungerstedt, U. 6-hydroxy-dopamine induced degeneration of central monoamine neurons. *Eur. J. Pharmacol.* **5**, (1968).

Vargas, M. R., Johnson, D. A., Sirkis, D. W., Messing, A. & Johnson, J. A. Nrf2 activation in astrocytes protects against neurodegeneration in mouse models of familial amyotrophic lateral sclerosis. *J. Neurosci.* **28**, (2008).

Vieira, L. B. *et al.* Inhibition of high voltage-activated calcium channels by spider toxin PnTx3-6. *J. Pharmacol. Exp. Ther.* **314**, (2005).

Voskuhl, R. R. *et al.* Reactive astrocytes form scar-like perivascular barriers to Silver, J. & Miller, J. H. Regeneration beyond the glial scar. *Nature Reviews Neuroscience* vol. 5 (2004).

Walsh, S., Finn, D. P. & Dowd, E. Time-course of nigrostriatal neurodegeneration and neuroinflammation in the 6-hydroxydopamine-induced axonal and terminal lesion models of Parkinson's disease in the rat. *Neuroscience* **175**, (2011).

Wanner, I. B. *et al.* Glial scar borders are formed by newly proliferated, elongated astrocytes that interact to corral inflammatory and fibrotic cells via STAT3-dependent mechanisms after spinal cord injury. *J. Neurosci.* **33**, (2013).

Yang, T., Dai, Y. J., Chen, G. & Cui, S. Sen. Dissecting the Dual Role of the Glial Scar and Scar-Forming Astrocytes in Spinal Cord Injury. Front. Cell. Neurosci. **14**, (2020).

Zhang, W. et al. 3-Hydroxymorphinan, a metabolite of dextromethorphan, protects nigrostriatal pathway against MPTP-elicited damage both in vivo and in vitro . FASEB J. **20**, (2006).

Ziv, Y. *et al.* Immune cells contribute to the maintenance of neurogenesis and spatial learning abilities in adulthood. *Nat. Neurosci.* **9**, (2006).

ATTACHMENTS

SUPPLEMENTARY MATERIAL

Supplementary Figure 1.

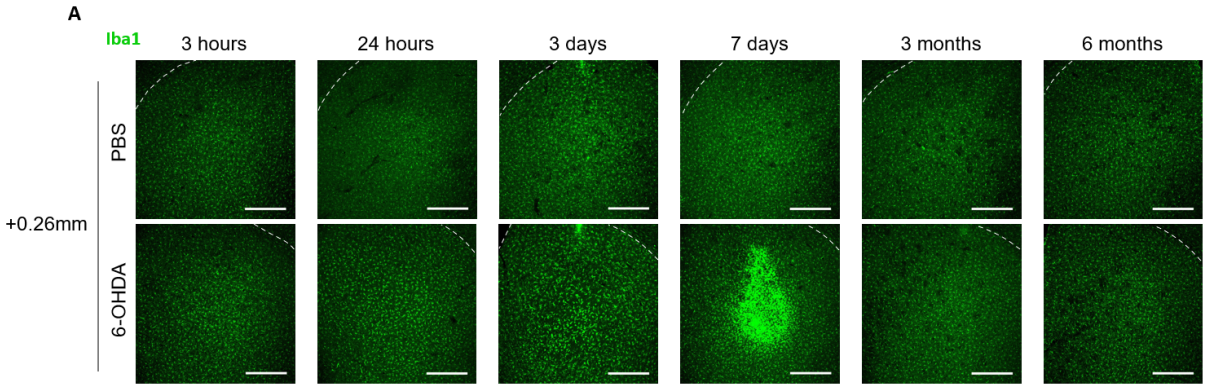

Supplementary Figure 1. AP coordinate +0.26mm representative coronal fluorescent images of microglial response to dopaminergic neurodegeneration in the dorsal striatum. **(A)** Representative coronal images of microglia (Iba1^{+}) in the dorsal striatum, showing the PBS-injected (top) and 6-OHDA-injected (bottom) hemispheres of the AP coordinate +0.26 in the 3 hour-group, 24 hour-group, 3 day-group, 7 day-group, 3 month-group, and 6 month-group. LV: Lateral Ventricle.

Supplementary Figure 2.

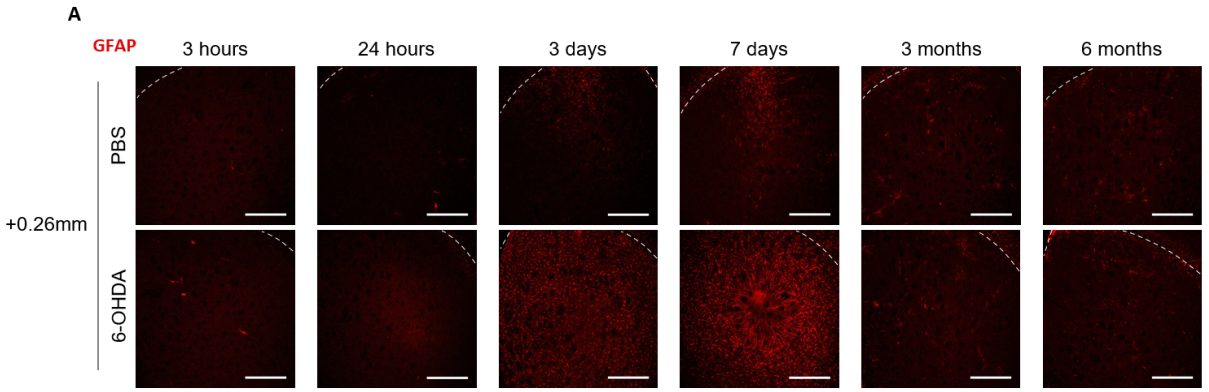

Supplementary Figure 2. AP coordinate +0.26mm representative coronal fluorescent images of astrocyte response to dopaminergic neurodegeneration in the dorsal striatum. (A) Representative coronal images of astrocyte (GFAP^{+}) in the dorsal striatum, showing the PBS-injected (top) and 6-OHDA-injected (bottom) hemispheres of the AP coordinate +0.26 in the 3 hour-group, 24 hour-group, 3 day-group, 7 day-group, 3 month-group, and 6 month-group. LV: Lateral Ventricle.

Supplementary tables 1 - Microglial reaction to 6-OHDA or PBS injection on striatal subregions

Tables 1.1 - Microglia reaction at AP coordinate +0.86mm

AP +0.86mm *	Mean Difference	95% CI	$q_{(26)}$	Summary	*p* value
3h vs. 24h	-0.07309	-0.1402 to -0.005953	3.339	*	0.0255
3h vs. 3d	-0.06820	-0.1353 to -0.001066	3.116	*	0.0444
3h vs. 3m	0.04867	-0.02385 to 0.1212	2.058	ns	0.4971
3h vs. 6m	0.08969	0.01717 to 0.1622	3.793	**	0.0080
24h vs. 3d	0.004887	-0.06225 to 0.07203	0.2233	ns	>0.9999
24h vs. 3m	0.1218	0.04924 to 0.1943	5.149	***	0.0002
24h vs. 6m	0.1628	0.09027 to 0.2353	6.884	****	<0.0001
3d vs. 3m	0.1169	0.04436 to 0.1894	4.943	***	0.0004
3d vs. 6m	0.1579	0.08538 to 0.2304	6.678	****	<0.0001
3m vs. 6m	0.04102	-0.03650 to 0.1185	1.623	ns	>0.9999

* 6-OHDA injected hemisphere

Table 1.1.1 - Microglial reaction to 6-OHDA at AP +0.86mm striatal coordinate between time points.

Table showing the statistical results of Tukey's multiple comparison test demonstrating the difference between the number of microglia, in the hemisphere that received 6-OHDA, between the groups. Data correspondent to **Figure 2G**.

AP +0.86mm *	Mean Difference	95% CI	$q_{(26)}$	Summary	*p* value
3h vs. 24h	-0.004771	-0.07191 to 0.06237	0.2180	ns	>0.9999
3h vs. 3d	0.01312	-0.05402 to 0.08026	0.5993	ns	>0.9999
3h vs. 3m	0.09076	0.01824 to 0.1633	3.838	**	0.0071
3h vs. 6m	0.1213	0.04879 to 0.1938	5.130	***	0.0002
24h vs. 3d	0.01789	-0.04925 to 0.08503	0.8173	ns	>0.9999
24h vs. 3m	0.09553	0.02301 to 0.1680	4.040	**	0.0042
24h vs. 6m	0.1261	0.05356 to 0.1986	5.332	***	0.0001
3d vs. 3m	0.07764	0.005121 to 0.1502	3.283	*	0.0293
3d vs. 6m	0.1082	0.03567 to 0.1807	4.575	**	0.0010
3m vs. 6m	0.03055	-0.04698 to 0.1081	1.209	ns	>0.9999

* PBS injected hemisphere

Table 1.1.2 - Microglial reaction to PBS at AP +0.86mm striatal coordinate between time points.

Table showing the statistical results of Tukey's multiple comparison test demonstrating the difference between the microglia number, in the hemisphere that received PBS, between the groups. Data correspondent to **Figure 2G**.

Tables 1.2 Microglia reaction at AP coordinate +0.50mm

AP +0.50mm *	Mean Difference	95% CI	$q_{(26)}$	Summary	*p* value
3h vs. 24h	-0.04545	-0.1377 to 0.04679	2.041	ns	0.6067
3h vs. 3d	-0.02248	-0.1147 to 0.06976	1.009	ns	0.9515
3h vs. 3m	0.09509	-0.004551 to 0.1947	3.952	ns	0.0667
3h vs. 6m	0.1150	0.01535 to 0.2146	4.779	*	0.0179
24h vs. 3d	0.02297	-0.06928 to 0.1152	1.031	ns	0.9477
24h vs. 3m	0.1405	0.04090 to 0.2402	5.842	**	0.0028
24h vs. 6m	0.1604	0.06080 to 0.2601	6.669	***	0.0006
3d vs. 3m	0.1176	0.01793 to 0.2172	4.887	*	0.0149
3d vs. 6m	0.1375	0.03783 to 0.2371	5.714	**	0.0035
3m vs. 6m	0.01990	-0.08662 to 0.1264	0.7737	ns	0.9813

* 6-OHDA injected hemisphere

Table 1.2.1 - Microglial reaction to 6-OHDA at AP +0.50mm striatal coordinate between time points.

Table showing the statistical results of Tukey's multiple comparison test demonstrating the difference between the microglia number, in the hemisphere that received 6-OHDA, between the groups. Data correspondent to **Figure 2H**.

AP +0.50mm *	Mean Difference	95% CI	$q_{(26)}$	Summary	*p* value
3h vs. 24h	0.02602	-0.06622 to 0.1183	1.168	ns	0.9201
3h vs. 3d	0.04767	-0.04458 to 0.1399	2.140	ns	0.5635
3h vs. 3m	0.1002	0.0005293 to 0.1998	4.163	*	0.0483
3h vs. 6m	0.1281	0.02846 to 0.2277	5.324	**	0.0070
24h vs. 3d	0.02164	-0.07061 to 0.1139	0.9716	ns	0.9575
24h vs. 3m	0.07414	-0.02550 to 0.1738	3.082	ns	0.2190
24h vs. 6m	0.1021	0.002436 to 0.2017	4.243	*	0.0427
3d vs. 3m	0.05250	-0.04714 to 0.1521	2.182	ns	0.5452
3d vs. 6m	0.08043	-0.01921 to 0.1801	3.343	ns	0.1574
3m vs. 6m	0.02793	-0.07859 to 0.1344	1.086	ns	0.9375

* PBS injected hemisphere

Table 1.2.2 - Microglial reaction to PBS at AP +0.50mm striatal coordinate between time points.

Table showing the statistical results of Tukey's multiple comparison test demonstrating the difference between the microglia number, in the hemisphere that received PBS, between the groups. Data correspondent to **Figure 2H**.

Tables 1.3 Microglia reaction at AP coordinate +0.26mm

AP +0.26mm *	Mean Difference	95% CI	$q_{(26)}$	Summary	*p* value
3h vs. 24h	-0.05397	-0.1468 to 0.03884	2.408	ns	0.4496
3h vs. 3d	-0.05085	-0.1437 to 0.04195	2.269	ns	0.5078
3h vs. 3m	0.03569	-0.06455 to 0.1359	1.474	ns	0.8332
3h vs. 6m	0.03569	-0.06455 to 0.1359	1.474	ns	0.8332
24h vs. 3d	0.003117	-0.08969 to 0.09592	0.1391	ns	>0.9999
24h vs. 3m	0.08966	-0.01058 to 0.1899	3.704	ns	0.0959
24h vs. 6m	0.08966	-0.01058 to 0.1899	3.704	ns	0.0959
3d vs. 3m	0.08654	-0.01370 to 0.1868	3.575	ns	0.1150
3d vs. 6m	0.08654	-0.01370 to 0.1868	3.575	ns	0.1150
3m vs. 6m	0.000	-0.1072 to 0.1072	0.000	ns	>0.9999

* 6-OHDA injected hemisphere

Table 1.3.1 - Microglial reaction to 6-OHDA at AP +0.26mm striatal coordinate between time points.

Table showing the statistical results of Tukey's multiple comparison test demonstrating the difference between the microglia number, in the hemisphere that received 6-OHDA, between the groups. Data correspondent to **Figure 2I**.

AP +0.26mm *	Mean Difference	95% CI	$q_{(26)}$	Summary	*p* value
3h vs. 24h	0.03169	-0.07775 to 0.1079	0.6717	ns	0.9890
3h vs. 3d	0.03169	-0.06345 to 0.1222	1.310	ns	0.8841
3h vs. 3m	0.03423	-0.06172 to 0.1388	1.592	*	0.7918
3h vs. 6m	0.03423	-0.02471 to 0.1758	3.120	**	0.2089
24h vs. 3d	0.03169	-0.07850 to 0.1071	0.6384	ns	0.9909
24h vs. 3m	0.03423	-0.07677 to 0.1237	0.9697	ns	0.9578
24h vs. 6m	0.03423	-0.03976 to 0.1607	2.499	*	0.4133
3d vs. 3m	0.03423	-0.09108 to 0.1094	0.3786	ns	0.9988
3d vs. 6m	0.03423	-0.05407 to 0.1464	1.908	ns	0.6642
3m vs. 6m	0.03659	-0.07015 to 0.1442	1.430	ns	0.8478

* PBS injected hemisphere

Table 1.3.2 - Microglial reaction to PBS at AP +0.26mm striatal coordinate between time points.

Table showing the statistical results of Tukey's multiple comparison test demonstrating the difference between the microglia number, in the hemisphere that received PBS, between the groups. Data correspondent to **Figure 2I**.

Tables 1.4 Microglia reaction at AP coordinate +0.14mm

AP +0.14mm *	Mean Difference	95% CI	$q_{(20)}$	Summary	*p* value
3h vs. 24h	-0.03865	-0.1434 to 0.06611	1.460	ns	0.7327
3h vs. 3m	0.04644	-0.06671 to 0.1596	1.624	ns	0.6647
3h vs. 6m	0.08833	-0.02482 to 0.2015	3.090	ns	0.1616
24h vs. 3m	0.08508	-0.02807 to 0.1982	2.976	ns	0.1857
24h vs. 6m	0.1270	0.01383 to 0.2401	4.442	*	0.0244
3m vs. 6m	0.04190	-0.07906 to 0.1629	1.371	ns	0.7680

* 6-OHDA injected hemisphere

Table 1.4.1 - Microglial reaction to 6-OHDA at AP +0.14mm striatal coordinate between time points.

Table showing the statistical results of Tukey's multiple comparison test demonstrating the difference between the microglia number, in the hemisphere that received 6-OHDA, between the groups. Data correspondent to **Figure 2J**.

AP +0.14mm *	Mean Difference	95% CI	$q_{(20)}$	Summary	*p* value
3h vs. 24h	-0.003805	-0.1086 to 0.1010	0.1438	ns	0.9996
3h vs. 3m	0.08436	-0.02879 to 0.1975	2.951	ns	0.1914
3h vs. 6m	0.09501	-0.01814 to 0.2082	3.324	ns	0.1200
24h vs. 3m	0.08816	-0.02499 to 0.2013	3.084	ns	0.1628
24h vs. 6m	0.09881	-0.01434 to 0.2120	3.457	ns	0.1006
3m vs. 6m	0.01065	-0.1103 to 0.1316	0.3485	ns	0.9946

* PBS injected hemisphere

Table 1.4.2 - Microglial reaction to PBS at AP +0.14mm striatal coordinate between time points.

Table showing the statistical results of Tukey's multiple comparison test demonstrating the difference between the microglia number, in the hemisphere that received PBS, between the groups. Data correspondent to **Figure 2J**.

Tables 1.5 Microglia reaction at AP coordinate -0.22mm

AP -0.22mm *	Mean Difference	95% CI	$q_{(20)}$	Summary	*p* value
3h vs. 24h	0.01142	-0.08999 to 0.1128	0.4457	ns	0.9888
3h vs. 3m	0.02310	-0.08644 to 0.1326	0.8346	ns	0.9339
3h vs. 6m	0.07302	-0.03651 to 0.1826	2.639	ns	0.2737
24h vs. 3m	0.01168	-0.09786 to 0.1212	0.4220	ns	0.9905
24h vs. 6m	0.06160	-0.04793 to 0.1711	2.226	ns	0.4149
3m vs. 6m	0.04993	-0.06717 to 0.1670	1.688	ns	0.6379

* 6-OHDA injected hemisphere

Table 1.5.1 - Microglial reaction to 6-OHDA at AP -0.22mm striatal coordinate between time points.

Table showing the statistical results of Tukey's multiple comparison test demonstrating the difference between the microglia number, in the hemisphere that received 6-OHDA, between the groups. Data correspondent to **Figure 2K**.

AP -0.22mm *	Mean Difference	95% CI	$q_{(20)}$	Summary	*p* value
3h vs. 24h	-0.02051	-0.1219 to 0.08090	0.8007	ns	0.9410
3h vs. 3m	0.1230	0.01344 to 0.2325	4.444	*	0.0243
3h vs. 6m	0.1556	0.04608 to 0.2651	5.624	**	0.0038
24h vs. 3m	0.1435	0.03395 to 0.2530	5.185	**	0.0077
24h vs. 6m	0.1761	0.06659 to 0.2857	6.365	**	0.0012
3m vs. 6m	0.03264	-0.08445 to 0.1497	1.103	ns	0.8625

* PBS injected hemisphere

Table 1.5.2 - Microglial reaction to PBS at AP -0.22mm striatal coordinate between time points.

Table showing the statistical results of Tukey's multiple comparison test demonstrating the difference between the microglia number, in the hemisphere that received PBS, between the groups. Data correspondent to **Figure 2K**.

Supplementary tables 2 - Microglia reaction to 6-OHDA or PBS on the average of all striatal subregions analysed

Tables 2.1 - Microglial reaction to 6-OHDA at average of AP coordinate +0.86mm to -0.22mm

AP +0.86mm - -0.22mm *	Mean Difference	95% CI	$q_{(36)}$	Summary	*p* value
3h vs. 24h	-0.03995	-0.08535 to 0.005452	3.572	ns	0.1072
3h vs. 3d	-0.04581	-0.09823 to 0.006617	3.547	ns	0.1112
3h vs. 3m	0.04980	0.004395 to 0.09520	4.453	*	0.0256
3h vs. 6m	0.08034	0.03494 to 0.1257	7.185	***	0.0001
24h vs. 3d	-0.005858	-0.05828 to 0.04657	0.4537	ns	0.9976
24h vs. 3m	0.08974	0.04434 to 0.1351	8.025	****	<0.0001
24h vs. 6m	0.1203	0.07489 to 0.1657	10.76	****	<0.0001
3d vs. 3m	0.09560	0.04318 to 0.1480	7.404	****	<0.0001
3d vs. 6m	0.1262	0.07373 to 0.1786	9.770	****	<0.0001
3m vs. 6m	0.03055	-0.01485 to 0.07595	2.732	ns	0.3196

* 6-OHDA injected hemisphere

Table 2.1.1 - Microglial reaction to 6-OHDA at average of AP +0.86mm to -0.22mm striatal coordinate between time points.

Table showing the statistical results of Tukey's multiple comparison test demonstrating the difference between the microglia number, in the hemisphere that received 6-OHDA, between the groups. Data correspondent to **Figure 2L**.

AP +0.86mm - -0.22mm *	Mean Difference	95% CI	$q_{(36)}$	Summary	*p* value
3h vs. 24h	0.002397	-0.04300 to 0.04780	0.2144	ns	0.9999
3h vs. 3d	0.02458	-0.02784 to 0.07700	1.904	ns	0.6649
3h vs. 3m	0.08736	0.04195 to 0.1328	7.812	****	<0.0001
3h vs. 6m	0.1151	0.06971 to 0.1605	10.29	****	<0.0001
24h vs. 3d	0.02218	-0.03024 to 0.07461	1.718	ns	0.7429
24h vs. 3m	0.08496	0.03956 to 0.1304	7.597	****	<0.0001
24h vs. 6m	0.1127	0.06731 to 0.1581	10.08	****	<0.0001
3d vs. 3m	0.06277	0.01035 to 0.1152	4.862	*	0.0122
3d vs. 6m	0.09053	0.03811 to 0.1430	7.011	***	0.0002
3m vs. 6m	0.02776	-0.01764 to 0.07316	2.482	ns	0.4146

* PBS injected hemisphere

Table 2.1.2 - Microglial reaction to PBS at average of AP +0.86mm to -0.22mm striatal coordinate between time points.

Table showing the statistical results of Tukey's multiple comparison test demonstrating the difference between the microglia number, in the hemisphere that received PBS, between the groups. Data correspondent to **Figure 2L**.

Supplementary tables 3 - Microglia reaction to 6-OHDA or PBS on the average of anterior striatal subregions

Tables 3.1 - Microglial reaction to 6-OHDA at average of AP coordinate +0.86mm to +0.26mm

AP +0.86mm - +0.26mm *	Mean Difference	95% CI	$q_{(26)}$	Summary	*p* value
3h vs. 24h	-0.05751	-0.1089 to -0.006062	4.630	*	0.0229
3h vs. 3d	-0.04718	-0.09862 to 0.004262	3.798	ns	0.0837
3h vs. 3m	0.05982	0.004251 to 0.1154	4.458	*	0.0303
3h vs. 6m	0.08012	0.02456 to 0.1357	5.972	**	0.0022
24h vs. 3d	0.01032	-0.04112 to 0.06177	0.8312	ns	0.9757
24h vs. 3m	0.1173	0.06176 to 0.1729	8.744	****	<0.0001
24h vs. 6m	0.1376	0.08206 to 0.1932	10.26	****	<0.0001
3d vs. 3m	0.1070	0.05143 to 0.1626	7.975	****	<0.0001
3d vs. 6m	0.1273	0.07174 to 0.1829	9.488	****	<0.0001
3m vs. 6m	0.02031	-0.03909 to 0.07971	1.416	ns	0.8524

* 6-OHDA injected hemisphere

Table 3.1.1 - Microglial reaction to 6-OHDA at average of AP +0.86mm to +0.26mm striatal coordinate between time points.

Table showing the statistical results of Tukey's multiple comparison test demonstrating the difference between the microglia number, in the hemisphere that received 6-OHDA, between the groups. Data correspondent to **Figure 2M**.

AP +0.86mm - +0.26mm *	Mean Difference	95% CI	$q_{(26)}$	Summary	*p* value
3h vs. 24h	0.01210	-0.03934 to 0.06354	0.9742	ns	0.9571
3h vs. 3d	0.03005	-0.02140 to 0.08149	2.419	ns	0.4452
3h vs. 3m	0.07648	0.02092 to 0.1320	5.701	**	0.0036
3h vs. 6m	0.1083	0.05275 to 0.1639	8.073	****	<0.0001
24h vs. 3d	0.01795	-0.03350 to 0.06939	1.445	ns	0.8431
24h vs. 3m	0.06438	0.008817 to 0.1199	4.799	*	0.0173
24h vs. 6m	0.09621	0.04065 to 0.1518	7.171	***	0.0003
3d vs. 3m	0.04644	-0.009130 to 0.1020	3.461	ns	0.1345
3d vs. 6m	0.07826	0.02270 to 0.1338	5.833	**	0.0029
3m vs. 6m	0.03183	-0.02757 to 0.09123	2.219	ns	0.5292

* PBS injected hemisphere

Table 3.1.2 - Microglial reaction to PBS at average of AP +0.86mm to +0.26mm striatal coordinate between time points.

Table showing the statistical results of Tukey's multiple comparison test demonstrating the difference between the microglia number, in the hemisphere that received PBS, between the groups. Data correspondent to **Figure 2M**.

Supplementary tables 4 - Astrocytes reaction to 6-OHDA or PBS injection on striatal subregions

Tables 4.1 - Astrocytes reaction at AP coordinate +0.86mm

AP +0.86mm *	Mean Difference	95% CI	$q_{(36)}$	Summary	*p* value
3h vs. 24h	-0.06442	-0.5514 to 0.4225	0.5629	ns	0.9986
3h vs. 3d	-0.6714	-1.158 to -0.1845	5.867	**	0.0025
3h vs. 7d	-1.163	-1.650 to -0.6761	10.16	****	<0.0001
3h vs. 3m	0.1181	-0.3688 to 0.6051	1.032	ns	0.9769
3h vs. 6m	0.002957	-0.4840 to 0.4899	0.02583	ns	>0.9999
24h vs. 3d	-0.6070	-1.094 to -0.1201	5.304	**	0.0075
24h vs. 7d	-1.099	-1.586 to -0.6117	9.600	****	<0.0001
24h vs. 3m	0.1826	-0.3044 to 0.6695	1.595	ns	0.8665
24h vs. 6m	0.06737	-0.4196 to 0.5543	0.5887	ns	0.9983
3d vs. 7d	-0.4916	-0.9786 to -0.004693	4.296	*	0.0467
3d vs. 3m	0.7896	0.3026 to 1.277	6.899	***	0.0003
3d vs. 6m	0.6744	0.1874 to 1.161	5.893	**	0.0024
7d vs. 3m	1.281	0.7943 to 1.768	11.19	****	<0.0001
7d vs. 6m	1.166	0.6791 to 1.653	10.19	****	<0.0001
3m vs. 6m	-0.1152	-0.6021 to 0.3717	1.007	ns	0.9793

* 6-OHDA injected hemisphere

Table 4.1.1 - Astrocytes reaction to 6-OHDA at AP +0.86mm striatal coordinate between time points.

Table showing the statistical results of Tukey's multiple comparison test demonstrating the difference between fluorescence intensity of astrocytes, in the hemisphere that received 6-OHDA, between the groups. Data correspondent to **Figure 3H**.

AP +0.86mm *	Mean Difference	95% CI	$q_{(36)}$	Summary	*p* value
3h vs. 24h	0.06018	-0.4268 to 0.5471	0.5258	ns	0.9990
3h vs. 3d	0.09060	-0.3963 to 0.5775	0.7917	ns	0.9930
3h vs. 7d	0.04586	-0.4411 to 0.5328	0.4007	ns	0.9997
3h vs. 3m	0.07757	-0.4094 to 0.5645	0.6778	ns	0.9966
3h vs. 6m	-0.03871	-0.5257 to 0.4482	0.3382	ns	0.9999
24h vs. 3d	0.03042	-0.4565 to 0.5174	0.2658	ns	>0.9999
24h vs. 7d	-0.01432	-0.5013 to 0.4726	0.1251	ns	>0.9999
24h vs. 3m	0.01739	-0.4695 to 0.5043	0.1520	ns	>0.9999
24h vs. 6m	-0.09889	-0.5858 to 0.3881	0.8640	ns	0.9895
3d vs. 7d	-0.04474	-0.5317 to 0.4422	0.3909	ns	0.9998
3d vs. 3m	-0.01303	-0.5000 to 0.4739	0.1139	ns	>0.9999
3d vs. 6m	-0.1293	-0.6163 to 0.3576	1.130	ns	0.9659
7d vs. 3m	0.03171	-0.4552 to 0.5187	0.2771	ns	>0.9999
7d vs. 6m	-0.08457	-0.5715 to 0.4024	0.7389	ns	0.9949
3m vs. 6m	-0.1163	-0.6032 to 0.3707	1.016	ns	0.9784

* PBS injected hemisphere

Table 4.1.2 - Astrocytes reaction to PBS at AP +0.86mm striatal coordinate between time points. Table showing the statistical results of Tukey's multiple comparison test demonstrating the difference between astrocytes fluorescence intensity, in the hemisphere that received PBS, between the groups. Data correspondent to **Figure 3H**.

Tables 4.2 - Astrocytes reaction at AP coordinate +0.50mm

AP +0.50mm *	Mean Difference	95% CI	$q_{(34)}$	Summary	*p* value
3h vs. 24h	-0.1569	-0.6894 to 0.3755	1.258	ns	0.9464
3h vs. 3d	-0.8318	-1.364 to -0.2994	6.668	***	0.0005
3h vs. 7d	-1.140	-1.645 to -0.6347	9.632	****	<0.0001
3h vs. 3m	0.07592	-0.4992 to 0.6510	0.5635	ns	0.9986
3h vs. 6m	-0.003093	-0.5782 to 0.5720	0.02295	ns	>0.9999
24h vs. 3d	-0.6749	-1.207 to -0.1424	5.410	**	0.0065
24h vs. 7d	-0.9829	-1.488 to -0.4778	8.306	****	<0.0001
24h vs. 3m	0.2329	-0.3422 to 0.8080	1.728	ns	0.8231
24h vs. 6m	0.1538	-0.4213 to 0.7290	1.142	ns	0.9642
3d vs. 7d	-0.3081	-0.8132 to 0.1971	2.603	ns	0.4545
3d vs. 3m	0.9077	0.3326 to 1.483	6.737	***	0.0005
3d vs. 6m	0.8287	0.2536 to 1.404	6.151	**	0.0015
7d vs. 3m	1.216	0.6659 to 1.766	9.437	****	<0.0001
7d vs. 6m	1.137	0.5869 to 1.687	8.824	****	<0.0001
3m vs. 6m	-0.07901	-0.6938 to 0.5358	0.5486	ns	0.9988

* 6-OHDA injected hemisphere

Table 4.2.1 - Astrocytes reaction to 6-OHDA at AP +0.50mm striatal coordinate between time points.

Table showing the statistical results of Tukey's multiple comparison test demonstrating the difference between fluorescence intensity of astrocytes, in the hemisphere that received 6-OHDA, between the groups. Data correspondent to **Figure 3I**.

AP +0.50mm *	Mean Difference	95% CI	$q_{(36)}$	Summary	*p* value
3h vs. 24h	0.05657	-0.4759 to 0.5890	0.4535	ns	0.9995
3h vs. 3d	0.1018	-0.4306 to 0.6343	0.8163	ns	0.9919
3h vs. 7d	-0.03675	-0.5419 to 0.4684	0.3105	ns	>0.9999
3h vs. 3m	0.06281	-0.5123 to 0.6379	0.4662	ns	0.9994
3h vs. 6m	-0.03007	-0.6052 to 0.5450	0.2232	ns	>0.9999
24h vs. 3d	0.04526	-0.4872 to 0.5777	0.3628	ns	0.9998
24h vs. 7d	-0.09332	-0.5984 to 0.4118	0.7886	ns	0.9931
24h vs. 3m	0.006248	-0.5689 to 0.5814	0.04637	ns	>0.9999
24h vs. 6m	-0.08664	-0.6617 to 0.4885	0.6430	ns	0.9973
3d vs. 7d	-0.1386	-0.6437 to 0.3665	1.171	ns	0.9602
3d vs. 3m	-0.03901	-0.6141 to 0.5361	0.2895	ns	>0.9999
3d vs. 6m	-0.1319	-0.7070 to 0.4432	0.9789	ns	0.9816
7d vs. 3m	0.09956	-0.4503 to 0.6495	0.7728	ns	0.9937
7d vs. 6m	0.006680	-0.5432 to 0.5566	0.05185	ns	>0.9999
3m vs. 6m	-0.09288	-0.7077 to 0.5219	0.6449	ns	0.9973

* PBS injected hemisphere

Table 4.2.2 - Astrocytes reaction to PBS at AP +0.50mm striatal coordinate between time points. Table showing the statistical results of Tukey's multiple comparison test demonstrating the difference between astrocytes fluorescence intensity, in the hemisphere that received PBS, between the groups. Data correspondent to **Figure 3I**.

Tables 4.3 - Astrocytes reaction at AP coordinate +0.26mm

AP +0.26mm *	Mean Difference	95% CI	$q_{(34)}$	Summary	*p* value
3h vs. 24h	-0.2488	-0.7824 to 0.2849	1.990	ns	0.7226
3h vs. 3d	-0.8420	-1.376 to -0.3083	6.734	***	0.0005
3h vs. 7d	-1.110	-1.617 to -0.6042	9.362	****	<0.0001
3h vs. 3m	-0.03547	-0.6119 to 0.5409	0.2627	ns	>0.9999
3h vs. 6m	-0.09154	-0.6680 to 0.4849	0.6779	ns	0.9966
24h vs. 3d	-0.5932	-1.127 to -0.05954	4.745	*	0.0221
24h vs. 7d	-0.8617	-1.368 to -0.3554	7.265	***	0.0002
24h vs. 3m	0.2133	-0.3631 to 0.7897	1.579	ns	0.8710
24h vs. 6m	0.1572	-0.4192 to 0.7336	1.164	ns	0.9611
3d vs. 7d	-0.2685	-0.7748 to 0.2378	2.264	ns	0.6037
3d vs. 3m	0.8065	0.2301 to 1.383	5.972	**	0.0022
3d vs. 6m	0.7504	0.1740 to 1.327	5.557	**	0.0049
7d vs. 3m	1.075	0.5238 to 1.626	8.325	****	<0.0001
7d vs. 6m	1.019	0.4678 to 1.570	7.891	****	<0.0001
3m vs. 6m	-0.05607	-0.6723 to 0.5601	0.3884	ns	0.9998

* 6-OHDA injected hemisphere

Table 4.3.1 - Astrocytes reaction to 6-OHDA at AP +0.26mm striatal coordinate between time points.

Table showing the statistical results of Tukey's multiple comparison test demonstrating the difference between fluorescence intensity of astrocytes, in the hemisphere that received 6-OHDA, between the groups. Data correspondent to **Figure 3J**.

AP +0.26mm *	Mean Difference	95% CI	$q_{(36)}$	Summary	*p* value
3h vs. 24h	0.08159	-0.4521 to 0.6153	0.6526	ns	0.9972
3h vs. 3d	0.06050	-0.4732 to 0.5942	0.4839	ns	0.9993
3h vs. 7d	-0.07279	-0.5791 to 0.4335	0.6137	ns	0.9979
3h vs. 3m	0.06006	-0.5164 to 0.6365	0.4447	ns	0.9996
3h vs. 6m	-0.02415	-0.6006 to 0.5523	0.1788	ns	>0.9999
24h vs. 3d	-0.02109	-0.5548 to 0.5126	0.1687	ns	>0.9999
24h vs. 7d	-0.1544	-0.6607 to 0.3519	1.302	ns	0.9385
24h vs. 3m	-0.02154	-0.5980 to 0.5549	0.1595	ns	>0.9999
24h vs. 6m	-0.1057	-0.6822 to 0.4707	0.7830	ns	0.9933
3d vs. 7d	-0.1333	-0.6396 to 0.3730	1.124	ns	0.9665
3d vs. 3m	-0.0004432	-0.5769 to 0.5760	0.003282	ns	>0.9999
3d vs. 6m	-0.08465	-0.6611 to 0.4918	0.6268	ns	0.9976
7d vs. 3m	0.1328	-0.4183 to 0.6840	1.029	ns	0.9771
7d vs. 6m	0.04864	-0.5025 to 0.5998	0.3767	ns	0.9998
3m vs. 6m	-0.08420	-0.7004 to 0.5320	0.5833	ns	0.9983

* PBS injected hemisphere

Table 4.3.2 - Astrocytes reaction to PBS at AP +0.26mm striatal coordinate between time points. Table showing the statistical results of Tukey's multiple comparison test demonstrating the difference between astrocytes fluorescence intensity, in the hemisphere that received PBS, between the groups. Data correspondent to **Figure 3J**.

Tables 4.4 - Astrocytes reaction at AP coordinate +0.14mm

AP +0.14mm *	Mean Difference	95% CI	$q_{(34)}$	Summary	*p* value
3h vs. 24h	-0.2874	-0.8736 to 0.2988	2.092	ns	0.6791
3h vs. 3d	-0.7364	-1.323 to -0.1501	5.362	**	0.0071
3h vs. 7d	-1.090	-1.646 to -0.5335	8.363	****	<0.0001
3h vs. 3m	-0.05176	-0.6849 to 0.5814	0.3489	ns	0.9999
3h vs. 6m	-0.3335	-0.9667 to 0.2997	2.248	ns	0.6107
24h vs. 3d	-0.4490	-1.035 to 0.1372	3.269	ns	0.2173
24h vs. 7d	-0.8022	-1.358 to -0.2461	6.157	**	0.0015
24h vs. 3m	0.2356	-0.3976 to 0.8688	1.588	ns	0.8684
24h vs. 6m	-0.04611	-0.6793 to 0.5871	0.3109	ns	>0.9999
3d vs. 7d	-0.3532	-0.9094 to 0.2029	2.711	ns	0.4096
3d vs. 3m	0.6846	0.05142 to 1.318	4.615	*	0.0278
3d vs. 6m	0.4029	-0.2303 to 1.036	2.716	ns	0.4077
7d vs. 3m	1.038	0.4324 to 1.643	7.317	***	0.0001
7d vs. 6m	0.7561	0.1507 to 1.362	5.331	**	0.0076
3m vs. 6m	-0.2817	-0.9586 to 0.3952	1.777	ns	0.8060

* 6-OHDA injected hemisphere

Table 4.4.1 - Astrocytes reaction to 6-OHDA at AP +0.14mm striatal coordinate between time points.

Table showing the statistical results of Tukey's multiple comparison test demonstrating the difference between fluorescence intensity of astrocytes, in the hemisphere that received 6-OHDA, between the groups. Data correspondent to **Figure 3K**.

AP +0.14mm *	Mean Difference	95% CI	$q_{(36)}$	Summary	*p* value
3h vs. 24h	0.02472	-0.5615 to 0.6109	0.1800	ns	>0.9999
3h vs. 3d	0.009131	-0.5771 to 0.5953	0.06648	ns	>0.9999
3h vs. 7d	-0.1369	-0.6930 to 0.4192	1.051	ns	0.9749
3h vs. 3m	0.02755	-0.6056 to 0.6607	0.1857	ns	>0.9999
3h vs. 6m	-0.06799	-0.7012 to 0.5652	0.4583	ns	0.9995
24h vs. 3d	-0.01559	-0.6018 to 0.5706	0.1135	ns	>0.9999
24h vs. 7d	-0.1616	-0.7177 to 0.3945	1.240	ns	0.9494
24h vs. 3m	0.002823	-0.6304 to 0.6360	0.01903	ns	>0.9999
24h vs. 6m	-0.09271	-0.7259 to 0.5405	0.6250	ns	0.9977
3d vs. 7d	-0.1460	-0.7021 to 0.4101	1.121	ns	0.9669
3d vs. 3m	0.01842	-0.6148 to 0.6516	0.1241	ns	>0.9999
3d vs. 6m	-0.07712	-0.7103 to 0.5561	0.5199	ns	0.9990
7d vs. 3m	0.1644	-0.4410 to 0.7699	1.159	ns	0.9618
7d vs. 6m	0.06889	-0.5365 to 0.6743	0.4857	ns	0.9993
3m vs. 6m	-0.09554	-0.7724 to 0.5814	0.6024	ns	0.9981

* PBS injected hemisphere

Table 4.4.2 - Astrocytes reaction to PBS at AP +0.14mm striatal coordinate between time points. Table showing the statistical results of Tukey's multiple comparison test demonstrating the difference between astrocytes fluorescence intensity, in the hemisphere that received PBS, between the groups. Data correspondent to **Figure 3K**.

Tables 4.5 - Astrocytes reaction at AP coordinate -0.22mm

AP -0.22mm *	Mean Difference	95% CI	$q_{(34)}$	Summary	*p* value
3h vs. 24h	-0.4353	-1.244 to 0.3729	2.299	ns	0.5880
3h vs. 3d	-1.240	-2.048 to -0.4314	6.547	***	0.0007
3h vs. 7d	-1.178	-1.945 to -0.4117	6.560	***	0.0007
3h vs. 3m	-0.4042	-1.277 to 0.4688	1.976	ns	0.7282
3h vs. 6m	-0.4181	-1.291 to 0.4550	2.044	ns	0.6998
24h vs. 3d	-0.8043	-1.613 to 0.003944	4.248	ns	0.0517
24h vs. 7d	-0.7432	-1.510 to 0.02363	4.137	ns	0.0619
24h vs. 3m	0.03114	-0.8419 to 0.9042	0.1523	ns	>0.9999
24h vs. 6m	0.01727	-0.8558 to 0.8903	0.08442	ns	>0.9999
3d vs. 7d	0.06117	-0.7056 to 0.8280	0.3405	ns	0.9999
3d vs. 3m	0.8355	-0.03756 to 1.708	4.085	ns	0.0673
3d vs. 6m	0.8216	-0.05144 to 1.695	4.017	ns	0.0749
7d vs. 3m	0.7743	-0.06048 to 1.609	3.959	ns	0.0819
7d vs. 6m	0.7604	-0.07435 to 1.595	3.888	ns	0.0913
3m vs. 6m	-0.01387	-0.9472 to 0.9194	0.06345	ns	>0.9999

* 6-OHDA injected hemisphere

Table 4.5.1 - Astrocytes reaction to 6-OHDA at AP -0.22mm striatal coordinate between time points.

Table showing the statistical results of Tukey's multiple comparison test demonstrating the difference between fluorescence intensity of astrocytes, in the hemisphere that received 6-OHDA, between the groups. Data correspondent to **Figure 3L**.

AP -0.22mm *	Mean Difference	95% CI	$q_{(36)}$	Summary	*p* value
3h vs. 24h	0.02018	-0.7881 to 0.8285	0.1066	ns	>0.9999
3h vs. 3d	-0.1796	-0.9879 to 0.6286	0.9487	ns	0.9840
3h vs. 7d	-0.1042	-0.8710 to 0.6626	0.5802	ns	0.9984
3h vs. 3m	0.0006742	-0.8724 to 0.8737	0.003297	ns	>0.9999
3h vs. 6m	-0.09295	-0.9660 to 0.7801	0.4544	ns	0.9995
24h vs. 3d	-0.1998	-1.008 to 0.6084	1.055	ns	0.9745
24h vs. 7d	-0.1244	-0.8912 to 0.6424	0.6926	ns	0.9962
24h vs. 3m	-0.01951	-0.8925 to 0.8535	0.09539	ns	>0.9999
24h vs. 6m	-0.1131	-0.9862 to 0.7599	0.5531	ns	0.9987
3d vs. 7d	0.07542	-0.6914 to 0.8422	0.4198	ns	0.9997
3d vs. 3m	0.1803	-0.6927 to 1.053	0.8816	ns	0.9885
3d vs. 6m	0.08670	-0.7863 to 0.9597	0.4239	ns	0.9996
7d vs. 3m	0.1049	-0.7299 to 0.9397	0.5364	ns	0.9989
7d vs. 6m	0.01128	-0.8235 to 0.8461	0.05769	ns	>0.9999
3m vs. 6m	-0.09362	-1.027 to 0.8397	0.4282	ns	0.9996

* PBS injected hemisphere

Table 4.5.2 - Astrocytes reaction to PBS at AP -0.22mm striatal coordinate between time points.

Table showing the statistical results of Tukey's multiple comparison test demonstrating the difference between astrocytes fluorescence intensity, in the hemisphere that received PBS, between the groups. Data correspondent to **Figure 3L**.

Supplementary tables 5 - Astrocytes reaction to 6-OHDA or PBS on all striatal subregions analysed

Tables 5.1 - Astrocytes reaction to 6-OHDA at average of AP coordinate +0.86mm to -0.22mm

AP +0.86mm - -0.22mm *	Mean Difference	95% CI	$q_{(34)}$	Summary	*p* value
3h vs. 24h	-0.2386	-0.4882 to 0.01108	4.079	ns	0.0679
3h vs. 3d	-0.8642	-1.114 to -0.6146	14.78	****	<0.0001
3h vs. 7d	-1.136	-1.373 to -0.8995	20.48	****	<0.0001
3h vs. 3m	-0.05947	-0.3291 to 0.2102	0.9414	ns	0.9845
3h vs. 6m	-0.1686	-0.4383 to 0.1010	2.670	ns	0.4267
24h vs. 3d	-0.6257	-0.8753 to -0.3760	10.70	****	<0.0001
24h vs. 7d	-0.8977	-1.135 to -0.6609	16.18	****	<0.0001
24h vs. 3m	0.1791	-0.09055 to 0.4487	2.835	ns	0.3608
24h vs. 6m	0.06992	-0.1997 to 0.3396	1.107	ns	0.9686
3d vs. 7d	-0.2721	-0.5089 to -0.03522	4.903	*	0.0167
3d vs. 3m	0.8048	0.5351 to 1.074	12.74	****	<0.0001
3d vs. 6m	0.6956	0.4260 to 0.9652	11.01	****	<0.0001
7d vs. 3m	1.077	0.8190 to 1.335	17.83	****	<0.0001
7d vs. 6m	0.9677	0.7098 to 1.225	16.02	****	<0.0001
3m vs. 6m	-0.1092	-0.3974 to 0.1791	1.617	ns	0.8598

* 6-OHDA injected hemisphere

Table 5.1.1 - Astrocytes reaction to 6-OHDA at average of AP +0.86mm to -0.22mm striatal coordinate between time points.

Table showing the statistical results of Tukey's multiple comparison test demonstrating the difference between fluorescence intensity of astrocytes, in the hemisphere that received 6-OHDA, between the groups. Data correspondent to **Figure 3M**.

AP +0.86mm - -0.22mm *	Mean Difference	95% CI	$q_{(34)}$	Summary	*p* value
3h vs. 24h	0.04865	-0.2010 to 0.2983	0.8318	ns	0.9912
3h vs. 3d	0.01648	-0.2332 to 0.2661	0.2818	ns	>0.9999
3h vs. 7d	-0.06096	-0.2978 to 0.1759	1.099	ns	0.9696
3h vs. 3m	0.04573	-0.2239 to 0.3154	0.7239	ns	0.9954
3h vs. 6m	-0.05077	-0.3204 to 0.2189	0.8037	ns	0.9925
24h vs. 3d	-0.03217	-0.2818 to 0.2175	0.5500	ns	0.9987
24h vs. 7d	-0.1096	-0.3464 to 0.1272	1.975	ns	0.7285
24h vs. 3m	-0.002917	-0.2726 to 0.2667	0.04618	ns	>0.9999
24h vs. 6m	-0.09942	-0.3691 to 0.1702	1.574	ns	0.8727
3d vs. 7d	-0.07744	-0.3143 to 0.1594	1.396	ns	0.9190
3d vs. 3m	0.02925	-0.2404 to 0.2989	0.4630	ns	0.9995
3d vs. 6m	-0.06725	-0.3369 to 0.2024	1.065	ns	0.9735
7d vs. 3m	0.1067	-0.1511 to 0.3645	1.766	ns	0.8096
7d vs. 6m	0.01019	-0.2476 to 0.2680	0.1686	ns	>0.9999
3m vs. 6m	-0.09650	-0.3848 to 0.1918	1.429	ns	0.9112

* PBS injected hemisphere

Table 5.1.2 - Astrocytes reaction to PBS at average of AP +0.86mm to -0.22mm striatal coordinate between time points.

Table showing the statistical results of Tukey's multiple comparison test demonstrating the difference between fluorescence intensity of astrocytes, in the hemisphere that received PBS, between the groups. Data correspondent to **Figure 3M**.

Supplementary tables 6 - Astrocytes reaction to 6-OHDA or PBS on the average of the anterior striatal subregions

Tables 6.1 - Astrocytes reaction to 6-OHDA at average of AP coordinate +0.86mm to +0.26mm

AP +0.86mm - +0.26mm *	Mean Difference	95% CI	$q_{(34)}$	Summary	*p* value
3h vs. 24h	-0.1567	-0.2469 to -0.06651	7.416	***	0.0001
3h vs. 3d	-0.7817	-0.8719 to -0.6915	36.99	****	<0.0001
3h vs. 7d	-1.138	-1.223 to -1.052	56.75	****	<0.0001
3h vs. 3m	0.05286	-0.04456 to 0.1503	2.316	ns	0.5804
3h vs. 6m	-0.03056	-0.1280 to 0.06687	1.339	ns	0.9312
24h vs. 3d	-0.6250	-0.7152 to -0.5348	29.58	****	<0.0001
24h vs. 7d	-0.9811	-1.067 to -0.8955	48.94	****	<0.0001
24h vs. 3m	0.2096	0.1121 to 0.3070	9.182	****	<0.0001
24h vs. 6m	0.1261	0.02872 to 0.2236	5.527	**	0.0052
3d vs. 7d	-0.3561	-0.4416 to -0.2705	17.76	****	<0.0001
3d vs. 3m	0.8346	0.7372 to 0.9320	36.56	****	<0.0001
3d vs. 6m	0.7512	0.6537 to 0.8486	32.91	****	<0.0001
7d vs. 3m	1.191	1.098 to 1.284	54.55	****	<0.0001
7d vs. 6m	1.107	1.014 to 1.200	50.73	****	<0.0001
3m vs. 6m	-0.08343	-0.1876 to 0.02073	3.419	ns	0.1788

* 6-OHDA injected hemisphere

Table 6.1.1 - Astrocytes reaction to 6-OHDA at average of AP +0.86mm to +0.26mm striatal coordinate between time points.

Table showing the statistical results of Tukey's multiple comparison test demonstrating the difference between fluorescence intensity of astrocytes, in the hemisphere that received 6-OHDA, between the groups. Data correspondent to **Figure 3N**.

AP +0.86mm - +0.26mm *	Mean Difference	95% CI	$q_{(26)}$	Summary	*p* value
3h vs. 24h	0.06611	-0.02409 to 0.1563	3.129	ns	0.2587
3h vs. 3d	0.08431	-0.005892 to 0.1745	3.990	ns	0.0781
3h vs. 7d	-0.02122	-0.1068 to 0.06435	1.059	ns	0.9741
3h vs. 3m	0.06681	-0.03061 to 0.1642	2.927	ns	0.3265
3h vs. 6m	-0.03097	-0.1284 to 0.06645	1.357	ns	0.9274
24h vs. 3d	0.01820	-0.07200 to 0.1084	0.8611	ns	0.9897
24h vs. 7d	-0.08734	-0.1729 to -0.001765	4.356	*	0.0432
24h vs. 3m	0.0007009	-0.09673 to 0.09813	0.03071	ns	>0.9999
24h vs. 6m	-0.09709	-0.1945 to 0.0003407	4.254	ns	0.0512
3d vs. 7d	-0.1055	-0.1911 to -0.01996	5.264	**	0.0086
3d vs. 3m	-0.01750	-0.1149 to 0.07993	0.7665	ns	0.9939
3d vs. 6m	-0.1153	-0.2127 to -0.01786	5.051	*	0.0127
7d vs. 3m	0.08804	-0.005121 to 0.1812	4.034	ns	0.0729
7d vs. 6m	-0.009750	-0.1029 to 0.08341	0.4467	ns	0.9995
3m vs. 6m	-0.09779	-0.2019 to 0.006367	4.008	ns	0.0760

* PBS injected hemisphere

Table 6.1.2 - Astrocytes reaction to PBS at average of AP +0.86mm to +0.26mm striatal coordinate between time points.

Table showing the statistical results of Tukey's multiple comparison test demonstrating the difference between fluorescence intensity of astrocytes, in the hemisphere that received PBS, between the groups. Data correspondent to **Figure 3N**.